ELSEVIER

Contents lists available at ScienceDirect

Quaternary Science Reviews

journal homepage: www.elsevier.com/locate/quascirev



Chironomid-based Holocene summer temperature dynamics from southern Spain

Gonzalo Jiménez-Moreno ^{a,*} , Narcís Prat ^b, Oliver Heiri ^c, Antonio García-Alix ^a , R. Scott Anderson ^d, Francisco J. Jiménez-Espejo ^e , Jon Camuera ^e, Charo López-Blanco ^a

- ^a Department of Stratigraphy and Paleontology, University of Granada, 18002, Granada, Spain
- ^b Freshwater Ecology and Management, Department of Ecology, University of Barcelona, Barcelona, Spain
- Geoecology, Department of Environmental Sciences, University of Basel, 4056, Basel, Switzerland
- ^d School of Earth & Sustainability, Northern Arizona University, Flagstaff, 86011, AZ, USA
- ^e Andalusian Earth Sciences Institute (IACT), Spanish Research Council (CSIC), 18100, Armilla, Granada, Spain

ARTICLE INFO

Handling Editor: P Rioual

Keywords: Chironomids Pollen Summer temperature Holocene Sierra Nevada Western Europe

ABSTRACT

Global warming is generating substantial environmental modifications in fragile alpine areas. Past temperature reconstructions are necessary to evaluate how climate change modified alpine environments before instrumental measurements. In this study, we present a reconstruction of Holocene mean July and summer air temperatures, derived from chironomid and pollen assemblages preserved in the sedimentary record from Laguna de la Mosca (LdlMo), an alpine lake located in the Sierra Nevada of southern Spain. The \sim 8500-year-long LdlMo record shows highest temperatures reached during the Early and Middle Holocene from \sim 8500 until \sim 7100 calibrated 14 C years BP (cal yr BP), when a first drop in temperatures occurred. Temperatures stabilized during the Middle Holocene and a second drop happened at \sim 4500 and 4200 cal yr BP, possibly associated with the 4.2 kyr climatic event. Temperatures remained generally low during the Late Holocene, interrupted by warming between 2300 and 1600 cal yr BP during the Iberian Roman Humid Period (IRHP), and around 1000 cal yr BP during the Medieval Climate Anomaly (MCA). Minimum temperatures are recorded during the end of the Little Ice Age (LIA) at \sim 1800 CE. A sudden and rapidly increasing trend in temperatures of \sim 2.5 $^{\circ}$ C occurred since 1955 CE related to anthropogenic climate warming. This study confirms the rapid recent warming at high elevations, affecting the very sensitive chironomid assemblages and compromising these fragile and unique alpine lake ecosystems.

1. Introduction

Reconstructing past temperature change is crucial for several reasons, as it provides invaluable insights into the Earth's climate system and assists in our understanding of current and future climate dynamics (IPCC et al., 2022). For example, the examination of past temperature changes permits the differentiation between climate variability caused by natural forcings (such as variations in Earth's orbit controlling insolation, volcanic eruptions, or solar variability), and anthropogenic changes (i.e., due to greenhouse gas concentrations) and helps to identify the underlying causes of observed climate patterns and trends (IPCC et al., 2022).

In addition, validation of climate models, which are essential tools for predicting future climate conditions, is accomplished by comparison against past climate data (IPCC et al., 2022). Accurate reconstructions of climate allow scientists to test the performance of these models and to refine them, leading to more reliable future climate projections. In this respect, reconstructions from proxy data, such as geochemistry, chironomid and pollen records from sediment cores, suggest that global temperatures peaked during the Early to Middle Holocene, approximately between 10,000–6000 cal yr BP, in a period often referred to as the "Holocene Thermal Maximum" (Kaufman et al., 2020). These reconstructions indicate a subsequent gradual cooling trend leading up to the pre-industrial era, with recent warming attributed to anthropogenic influences (Kaufman et al., 2020). However, climate models generally simulate a more continuous warming trend throughout the Holocene, driven by increasing greenhouse gas concentrations and other factors. These models do not always reproduce the Early Holocene temperature

E-mail address: gonzaloj@ugr.es (G. Jiménez-Moreno).

 $^{^{\}ast}$ Corresponding author.

peak and subsequent cooling observed in the proxy data. This model-data discrepancy is commonly referred to as the Holocene temperature conundrum (Liu et al., 2014).

Further, reconstructing past temperatures allows us to evaluate how ecosystems responded to previous climate changes. Such studies can offer insights into the resilience and adaptability of various species and ecosystems to changing climates, e.g., during the Holocene period, guiding conservation efforts. Finally, past climate data provide context for current climate change, highlighting the unprecedented nature of recent warming trends. This evidence is critical for policymakers to justify and design effective climate mitigation and adaptation strategies.

A number of chironomid-based summer temperature records covering the Holocene are now available from Europe. Some regions, such as the Alps (e.g. Heiri et al., 2015; Ilyashuk et al., 2011) or Scandinavia (e.g. Velle et al., 2005; Luoto et al., 2014) are represented by a relatively large number of records. However, only a few individual and widely distributed reconstructions are available from Southern Europe, e.g. from the Pyrenees (Tarrats et al., 2018), the Sierra Nevada (Jiménez-Moreno et al., 2023), the Apennines (Samartin et al., 2017), the Dinaric Alps (Schmidhauser et al., 2024) and the southern Carpathians (Toth et al., 2015), and only in some few cases have multiple records been produced from the same region to evaluate whether they record similar Holocene temperature trends (e.g. Samartin et al., 2017). Here, we present a detailed fossil chironomid analysis of the Laguna de la Mosca (LdlMo) composite sedimentary record (LdlMo-13), covering the past ~8500 years. The remains of chironomid larvae, primarily their chitinous head capsules, are well-preserved in Late Pleistocene and Holocene lake sediments from the Sierra Nevada (Jiménez-Moreno et al., 2023). These head capsules possess unique morphological characteristics that allow identification at the generic, species-group, or morphotype levels (Brooks et al., 2007). The Chironomidae from high mountain lakes in Spain were studied in a series of papers in late 20th century (Rieradevall et al., 1999; Rieradevall and Prat, 1999) in which the preferences for substrate and depth of each species were noted. Chironomid assemblages are also known to be sensitive to summer temperatures in continental environments (Brooks, 2006; Eggermont and Heiri, 2012), enabling the estimation of past summer temperature variability based on changes in species assemblages (Brooks and Birks, 2001; Samartin et al., 2017) and numerical chironomid – temperature inference models (transfer functions; e.g. Brooks and Birks, 2001; Heiri et al., 2011).

The main goal of this study is to generate a chironomid record from LdlMo-13 core, enabling the development of a quantitative summer temperature reconstruction for the Sierra Nevada region over the past 8500 years. Comparing this summer temperature record with a previously published pollen record from the same LdlMo-13 sediment core (Manzano et al., 2019), a summer temperature reconstruction from that pollen record (this study), and a chironomid-based quantitative summer temperature reconstruction from the Laguna de Río Seco in Sierra Nevada (Jiménez-Moreno et al., 2023), and other paleoclimate records refines our understanding of regional climate dynamics during the Holocene, assesses the extent to which recent climate warming exceeds this baseline variability, and evaluates the impacts of climatic change on the environment in this mountain area of southern Spain.

2. Sierra Nevada and LdlMo

The Sierra Nevada range is located in the southeastern Iberian Peninsula (Fig. 1) and stretches for 90 km in an east-west direction parallel to the Mediterranean coast. This mountain range is home to the highest mountains in the Iberian Peninsula with several peaks above 3000 m above sea level (m a.s.l.). The geology in the central and highest part of the range is dominated by metamorphic siliceous rocks, particularly mica schists (Díaz de Federico et al., 1997). During the last glacial

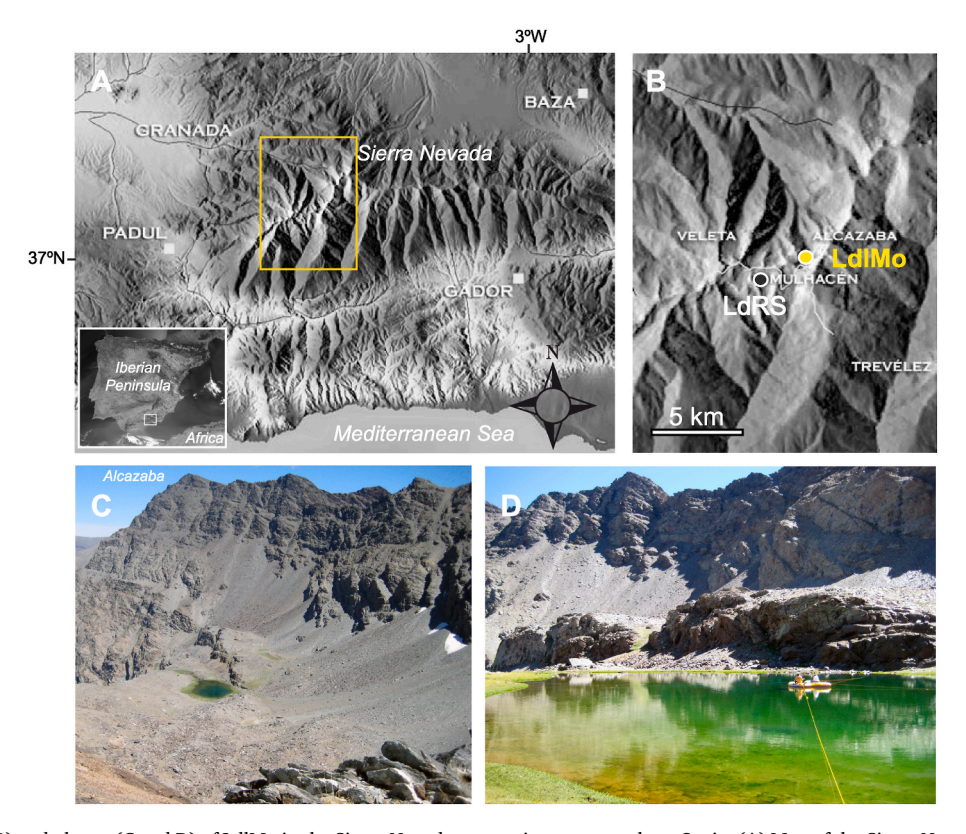


Fig. 1. Location (A and B) and photos (C and D) of LdlMo in the Sierra Nevada mountain range, southern Spain. (A) Map of the Sierra Nevada mountain range in the southern Iberian Peninsula. The rectangle shows the magnified area indicated in (B), where the main peaks and the LdlMo and the nearby Laguna de Río Seco (LdRS) lakes are located. (C) Photo of the LdlMo with the Alcazaba peak (3369 m a.s.l.) in the background. (D) Field photo of LdlMo with the coring platform situated at the lake center in September 2013.

maximum (LGM), Sierra Nevada was extensively glaciated. Evidences of LGM glaciers, spanning elevations of 2000–2200m a.s.l. on the north face and 2300–2400m a.s.l. on the south face, have been documented by Palacios et al. (2016). The subsequent melting of glaciers after deglaciation resulted in the formation of small lakes and peat bogs in the cirque basins, which are mostly located between 2500 and 3200m a.s.l.

The Laguna de la Mosca (LdlMo, 2897m a.s.l., 37°3.58′ N, 3°18.88′ W; Fig. 1) is a small alpine lake of glacial origin with a maximum depth of 3.4 m, a surface area of 0.48 ha, and a drainage area of 39.7 ha. Situated at the base of the north-facing Mulhacén cirque on metamorphic mica schists, the lake lies above the modern treeline within the cryoromediterranean (i.e., tundra) vegetation belt (Fig. 1). LdlMo has a continuous outflow of water throughout the summer. Only in extremely dry years and at the end of summer (e.g., 2005, 2015) has its effluent been observed to be dry. However, LdlMo has never been known to dry out completely and still retains water even under extreme drought conditions (https://lagunasdesierranevada.es/laguna-de-la-mosca/). The values of the water chemistry variables analyzed from Laguna de la Mosca characterize it as an oligotrophic system with low alkalinity waters (Pérez-Martínez et al., 2018).

Climate in the study area is Mediterranean, with hot and dry summers. The total annual rainfall at LdlMo is \sim 725 \pm 25 mm, with most of the precipitation (\sim 75 %) falling as snow due to the lake's elevation at ~2900m a.s.l. The mean annual temperature is approximately 4.4 °C, ranging from about -4 °C in the coldest month to around 18 °C in the warmest period, based on instrumental data from 1965 to 1993 CE at Prado Llano-Albergue University, located 15 km from the study site at an elevation of 2500m a.s.l. (Observatorio del cambio global de Sierra Nevada, 2020; Spanish National Weather Agency - AEMet Open Data, 2022). Direct summer air temperature measurements are not available for LdlMo. However, mean summer temperatures of 13 °C have been recorded at the south facing Laguna de Río Seco (Jiménez-Moreno et al., 2023), and 11.8 °C at the south facing Veleta peak (https://www.aemet. es/es/datos_abiertos/AEMET_OpenData), both located at a similar elevation but different exposition (south-facing instead of north-facing). LdlMo is generally covered by snow and ice from October to June, leaving an ice-free season that typically spans from June to October, though this duration can vary greatly from year to year. During the ice-free period, the lake receives meltwater and rainwater through temporary inlets (Fig. 1).

The present-day distribution of living larvae and head capsules of Chironomidae in LdlMo was investigated by Pérez-Martínez et al. (2018). In the littoral zone, as many as 10 chironomid species were recorded, whereas in the deepest zone this number was reduced by half, particularly in terms of concentration per gram of sediment. The littoral assemblages are dominated by *Corynoneura*, followed by *Psectrocladius* and *Micropsectra radialis*, while the deepest assemblages are dominated by *Micropsectra radialis*. The low diversity was attributed to the harsher environmental conditions at high elevation, including prolonged ice cover and low temperatures (Pérez-Martínez et al., 2018). The dominance of *Micropsectra radialis* and the occurrence of other taxa such as *Pseudodiamesa nivosa* were interpreted as reflecting the high-mountain and cold climate conditions at LdlMo (Pérez-Martínez et al., 2018).

3. Material and methods

In September 2013, two sediment cores were retrieved from the depocenter of the LdlMo lake bottom using a floating platform anchored to the shore. A 190-cm long sediment core (LdlMo-13-02) was collected with a Livingston corer, while a short 20-cm core (LdlMo-13-S) was sampled using a universal corer (Aquatic Research Inc.) to ensure an undisturbed sample of the less compacted upper sediment layers of the sedimentary sequence.

The LdlMo-13-02 core was transported to the University of Granada (UGR), where it was stored in a refrigerated room at 4 $^{\circ}$ C. Subsequently, the different drives were split and photographed in the laboratory at

UGR. The sediment characteristics of both LdlMo-13-02 and LdlMo-13-S cores were analyzed in detail, offering valuable insights into their composition (for more information, refer to Manzano et al., 2019, Fig. 2). Magnetic susceptibility (MS) measurements for core LdlMo-13-02 were also previously conducted using a Bartington MS2E meter, with readings recorded at 5 mm intervals along the entire core length (Fig. 2). MS measures the magnetic charge in the sediments (Snowball and Sandgren, 2001). However, MS analysis was not performed on core LdlMo-13-S because its sediments were sampled directly in the field and stored in plastic bags, which precluded further testing (Manzano et al., 2019, Fig. 2). Grain size distribution was previously analyzed by Manzano et al. (2019) in a total of 44 bulk sediment samples taken at 4 cm intervals throughout the sedimentary record (Fig. 2).

A total of 16 samples from the long sediment core were previously selected for AMS radiocarbon dating (Table 1; see Manzano et al., 2019). Bulk organic matter samples were considered for dating, since the bedrock does not contain carbonates and the lake represents a low-conductivity system. Incorporation of old carbon into algae and other aquatic biomass is therefore extremely unlikely. Additionally, a date corresponding to 1963 CE was derived from an ICP-MS Plutonium profile obtained from the upper 15 cm of the short core (Table 1; Manzano et al., 2019). In this study, the age model was updated with a new calibration of the radiocarbon dates using the IntCal20 calibration curve (Table 1; Reimer et al., 2020) and an updated Bayesian age-model that has been constructed using the OxCal 4.4 program (Bronk Ramsey, 2009). We selected a Poisson-process deposition model (P_Sequence function) and a general outlier model with a prior probability of 5 %. The new P sequence function model offer a better solution to link the obtained dates than in the previous age model by Manzano et al. (2019).

The organic elemental composition of the LdlMo-13 record was analyzed with the goal of obtaining information about the organic fraction within the bulk sediment (Fig. 3). A total of 177 samples, collected at approximately 1 cm intervals, were previously freeze-dried and then decarbonated overnight using acid digestion with 1 N HCl. Afterwards, they were rinsed and centrifuged with Milli-Q water until achieving a neutral pH, followed by another freeze-drying cycle. The elemental composition (C and N) of the decarbonated fraction was measured using an UNICUBE elemental analyzer at the Department of Stratigraphy and Paleontology at UGR. The difference in weight between the bulk and decarbonated samples was used to calculate the carbonate fraction's percentage in each sample. Total C and N contents were then recalculated based on the original bulk sediment weight. Atomic C/N ratios were determined from the total organic carbon (% TOC) and total nitrogen (%N) contents (Fig. 3).

Chironomid analysis was performed on 62 samples of 2 cm³ of sediment that were taken at different depths throughout the LdlMo-13-02 and LdlMo-13-S cores. The samples were previously treated with 10 % potassium hydroxide (KOH), resulting in the disaggregation of clays, which were then sieved using a 90-µm sieve. The material retained on the sieve was transferred to a Bogorov counting chamber and examined under a binocular microscope. All chironomid individuals present in each sample were extracted, transferred to microscope slides, and once dehydrated, mounted with Euparal. Chironomid head capsules were identified to morphotypes using a transmitted light microscope at 100x - 400x magnification with the aid of various guides (Wiederholm, 1983; Rieradevall and Brooks, 2001; Brooks et al., 2007). Chironomid relative abundances (%) were calculated with respect to the total chironomid count in each sample and were plotted using TILIA (Grimm, 1992) in a detailed diagram shown in Fig. 4.

Currently, no dedicated, local chironomid-temperature calibration dataset is available for southern European mountainous regions. Instead, for our mean July air temperature reconstruction (Fig. 5), we utilized the combined 274-lake chironomid-temperature calibration dataset and transfer function from the Swiss Alps and Norway. This dataset encompasses a broad range of elevations and temperature conditions in both regions, spans a mean July air temperature gradient from

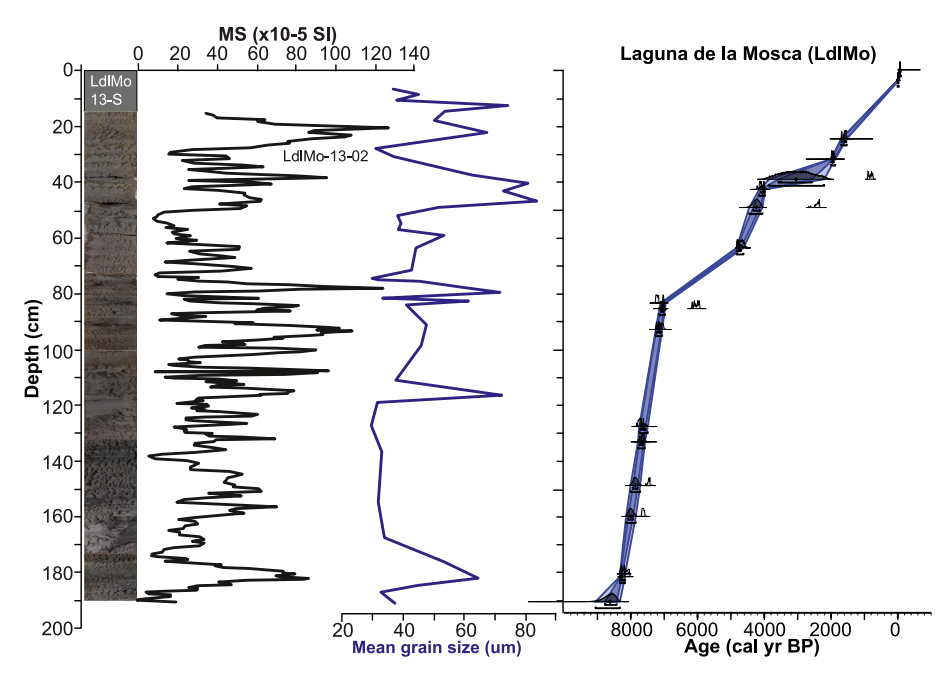


Fig. 2. Core photo, MS, mean grain size and updated Bayesian age-depth model for the LdlMo sediment record. Lithology and MS were previously described in Manzano et al. (2019). On the left, LdlMo-13-S stands for the short core and LdlMo-13-02 for the long Livingstone-recovered core, both taken in September 2013 (see details in Manzano et al., 2019). The Bayesian age-depth model was constructed using the OxCal 4.4 program (Bronk Ramsey, 2009). The blue area in the age-depth model represents the calibrated radiocarbon ages along with their uncertainties. (For interpretation of the references to colour in this figure legend, the reader is referred to the Web version of this article.)

Table 1
Radiometric ages from Laguna de la Mosca cores 13-S and 13-02. With an asterisk and in red is the single date that was rejected for the age model construction.
Radiocarbon ages were calibrated using the IntCal 20 calibration curve (Reimer et al., 2020).

Sample ID	Depth (cm)	Age (¹⁴ C yr BP)	¹⁴ C error	Calibrated age (cal yr BP) 2σ ranges	Median (cal yr BP)
Surf	0.0				-63
Pu	3.8				-13
D-AMS 005126	24.8	1700	29	1533–1695	1588
D-AMS 005127	32.1	2003	21	1881–1995	1943
D-AMS 004807	39.3	906	28	734–908	817
D-AMS 005128	43.0	3747	30	3985-4230	4107
D-AMS 005129	49.5	2375	34	2337-2669	2403
D-AMS 005130	64.0	4153	31	4577-4825	4698
D-AMS 005131*	77.8	29671	245	33691-34608	34204
D-AMS 005132	83.8	6275	40	7021–7277	7209
D-AMS 005133	85.8	5256	36	5929-6179	6036
D-AMS 005134	93.3	6229	42	7001–7255	7114
D-AMS 004379	128.1	6910	34	7671–7832	7735
D-AMS 004380	133.6	6785	43	7572–7686	7631
D-AMS 004381	149.3	6548	31	7368–7562	7460
D-AMS 004382	160.4	6791	41	7575–7685	7635
D-AMS 004383	181.0	7403	36	8046-8341	8252
D-AMS 004384	182.0	7334	38	8023-8111	8111

4 to 18.4 °C and samples a diverse range of arctic, alpine, subalpine, and temperate lakes (Heiri et al., 2011). Furthermore, it has previously been successfully applied to temperature reconstructions in southern European mountain lakes (Samartin et al., 2017; Tarrats et al., 2018; Jiménez et al., 2019; Jiménez-Moreno et al., 2023). All morphotypes identified in LdlMo are well represented within this dataset, particularly in samples from high-elevation lakes in the Alps. For reconstruction *Micropsectra contracta* type and *M. lindrothi* type were pooled with *M. insignilobus* type in the calibration data, as these *Micropsectra* types were not differentiated in the training set. Similarly, *Diamesa zernyi* type and *Diamesa* were pooled for reconstruction. The temperature reconstruction was conducted using the C2 program (version 1.7.6) (Juggins, 2014), applying a transfer function based on Weighted Averaging Partial Least Squares regression (WA-PLS; Ter Braak and Juggins, 1993; Ter Braak et al., 1993). This approach assumes a unimodal relationship between taxa

and climatic parameters and is robust to spatial autocorrelation (Telford and Birks, 2005). This method assumes that climate strongly influences the distribution and composition of the community as every species is characterized by distinct ranges of ecological tolerances. Performance statistics were calculated using cross-validation, including the coefficient of determination (R^2), the root mean square error of prediction (RMSEP), and the maximum bias. The model achieved a R^2 of 0.87 and RMSEP of 1.40 °C. The RMSEP, R^2 , and sample-specific errors of prediction (eSEPs) were calculated through 9999 bootstrapping cycles in C2. Individual samples in the LdlMo record were characterized by low chironomid concentrations and therefore low counts per sample. To reach an adequate count size for reconstruction adjacent low count samples were combined aiming for a minimum count of 40 chironomids per sample, although this could not be achieved in every case. The final pooled record for LdlMo for reconstruction resulted in 43 samples of

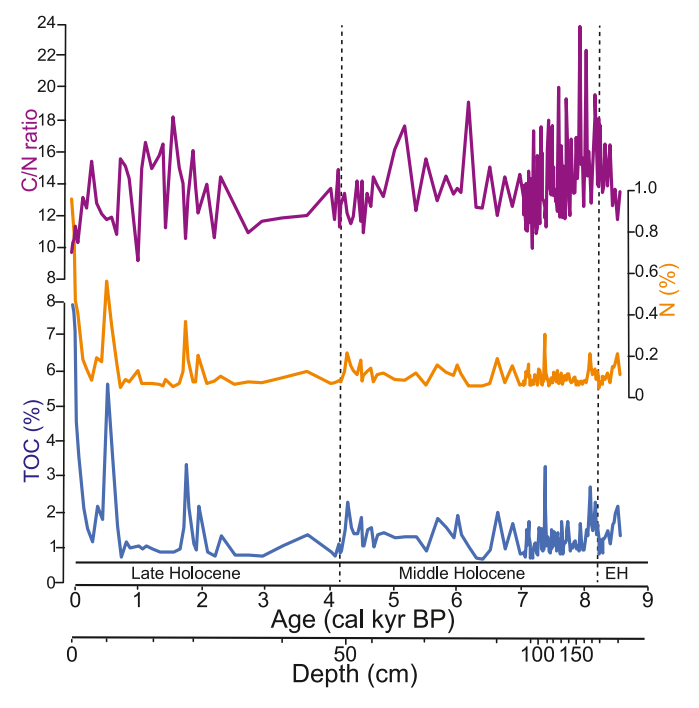


Fig. 3. Organic geochemistry data (from bottom to top TOC content, N and C/N) of the LdlMo sedimentary record. The duration of the Early (EH), Middle and Late Holocene is indicated with dashed vertical lines.

which 40 reached 39–204 counts, two only 25 counts and one 33 counts. Before applying WA-PLS, chironomid assemblage percentage data were square-root transformed to improve statistical robustness. To enhance model reliability, 19 sites with unusual hydrological or ecological conditions and high prediction residuals were identified as outliers and removed from the calibration data, following the approach described in Heiri et al. (2011). To assess the reliability of the transfer function approach, we evaluated the quality of modern analogues by comparing modern and fossil chironomid data (Birks et al., 1990). We used R studio 2024.09.0 with the "analogue" package (Simpson, 2007). For assessing the analogues situation we use the same thresholds established for pollen data and used for our pollen-based reconstruction (see below). A squared chord distance below the 5th percentile of all modern–fossil distances is considered to represent good analogues, whereas a distance above the 10th percentile suggests a no-analogue assemblage (Cao et al.,

2017). Our results show that all chironomid samples from LdlMo fall within the "good analogue" range, demonstrating a strong correspondence between fossil and modern samples (Supplementary Fig. 1).

The quantitative summer (June-July-August) temperature from LdlMo was also reconstructed using the pollen record (Manzano et al., 2019), which includes 75 fossil pollen samples from cores LdlMo-13-02 and LdlMo-13-S (Fig. 5). The modern pollen training set utilized in this quantitative estimation is based on the most recent version of the Eurasian Modern Pollen Database (EMPDv2) (Davis et al., 2020). The study area was constrained to a region exhibiting similar ecological characteristics and comparable vegetation responses to past climatic fluctuations. Therefore, we selected a region delimited by latitudes 25°N to 50°N and longitudes 15°W to 20°E. Moreover, since LdlMo is an alpine lake and to have a better signal of the high-elevation western Mediterranean/southern European vegetation in the modern dataset comparable to our record, we excluded low-elevation pollen sites (i.e. below 1500 m.a.s.l.), which resulted in 673 pollen samples. Taxonomic harmonization of both the modern pollen data (EMPDv2) and fossil pollen records was conducted by merging minor taxa and species with low relative abundances into broader taxonomic units (e.g., genera, families), resulting in a final dataset of 269 harmonized taxa. Recent temperature data were obtained from the WorldClim v2.1 database at a 30-s resolution. The quantitative temperature reconstruction of LdlMo was performed using the pollen-based transfer function technique, also using the WA-PLS calibrated regression model. We used the two-component WA-PLS model because increasing the number of components can lead to overfitting of the data, which in turn decreases the predictive value of the model. In this model, taxa are weighted according to their abundance and how well their distribution matches with the environmental gradient (ter Braak et al., 1993). To minimize data noise, a square-root transformation was also applied to the species data in the modern pollen training set. The reconstructions were performed using the C2 software (version 1.7.6) (Juggins, 2014). The performance of the WA-PLS regression model was assessed using a leave-one-out cross-validation approach (Birks et al., 1990). The performance statistics for the summer temperature reconstructions report a R^2 of 0.80, an RMSEP of 1.95 °C, and a maximum bias of 6.0 °C, whereas the annual temperature shows a R² of 0.78, an RMSEP of 1.94 °C, and a maximum bias of 6.41 °C. We also evaluated close analogue quality statistics for the pollen data to determine whether all fossil samples had sufficient analogues in the modern calibration dataset (see methodology for the chironomids above; Supplementary Fig. 2). The analysis shows that 42.6 % of fossil samples are classified as "good analogues," 28 % as "fair analogues," and 29.4 % as "no analogues." Although the analogue

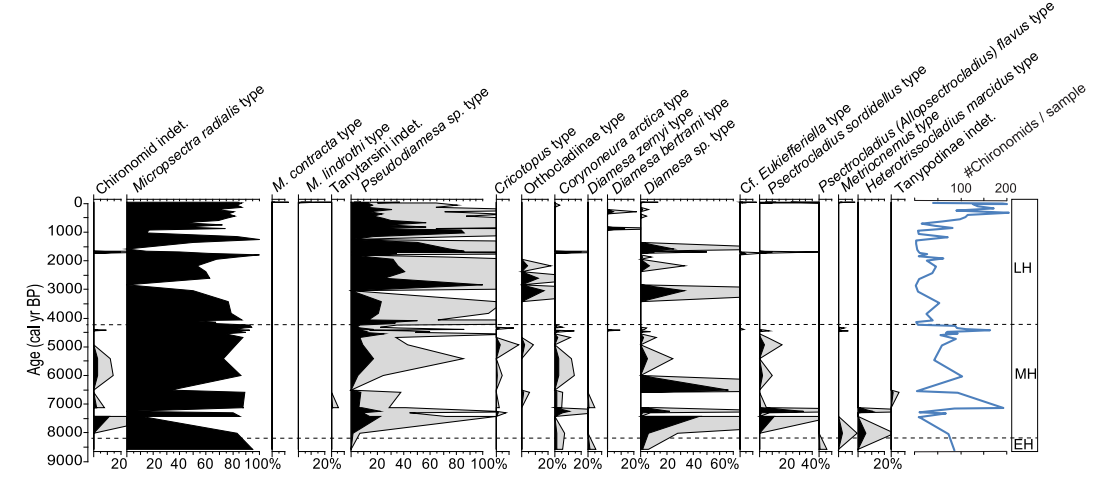


Fig. 4. Detailed diagram of chironomid assemblages changing over time in the LdlMo record. Shadings show 5x exaggeration. The chironomid concentration is shown with a blue line. The duration of the Early, Middle and Late Holocene (EH, MH and LH) is indicated on the right with dashed horizontal lines. (For interpretation of the references to colour in this figure legend, the reader is referred to the Web version of this article.)

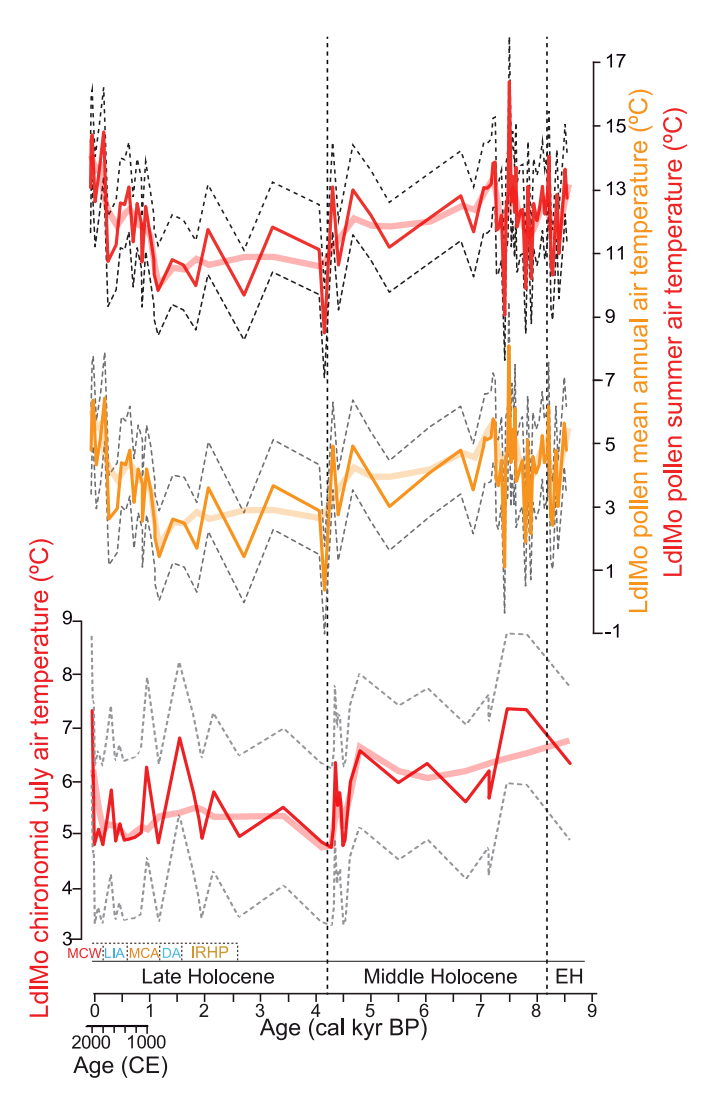


Fig. 5. Summer temperature reconstructions from LdlMo. At the bottom are the chironomid-inferred July air temperatures from the LdlMo composite record (solid red line) and associated estimated standard error of prediction (eSEP; black dashed lines) for each sample. In pink shading is a Loess smoothing (factor 0.2) of the raw chironomid temperature data calculated using Past4 software (Hammer et al., 2001). At the top is the pollen-inferred mean annual and summer (June, July and August) air temperatures from the LdlMo composite record (solid orange and red lines, respectively) and associated estimated standard error of prediction (eSEP; black dashed lines) for each sample. In pink shading is a Loess smoothing (factor 0.1) of the raw pollen temperature data calculated using Past4 software (Hammer et al., 2001). In the middle is the mean annual air temperature estimation using the pollen data, for comparison. In lighter orange is a Loess smoothing (factor 0.1) of the raw pollen temperature data calculated using Past4 software (Hammer et al., 2001). The duration of the Early (EH), Middle and Late Holocene is indicated with dashed vertical lines. IRHP, DA, MCA, LIA and MCW stand for Iberian Roman Humid Period, Dark Ages, Medieval Climate Anomaly, Little Ice Age and Modern Climate Warming. (For interpretation of the references to colour in this figure legend, the reader is referred to the Web version of this article.)

performance for pollen is weaker than for chironomids—and nearly one-third of pollen samples fall into the "no analogue" category—this does not imply that their temperature estimates are invalid. Instead, the quantitative results from these samples should be interpreted with caution. Notably, most of the no analogue samples occur within the last ~2000 years, likely reflecting the appearance of non-native species (e. g., cultivars, nitrophilous, and ruderal plants), as previously reported by Manzano et al. (2019) for the LdlMo pollen record, which differs from the modern training set.

Cladoceran resting eggs (e.g., *Daphnia* ephippia in Fig. 6), seed, and charcoal macroremains were previously extracted from 160 samples by deflocculating 1 cm 3 of sediment in tetrasodium pyrophosphate and sieving the material through 250 μ m and 125 μ m meshes by Manzano et al. (2019). Counting and identification of these macroremains in each sample were conducted under ~25x–50x magnifications. No

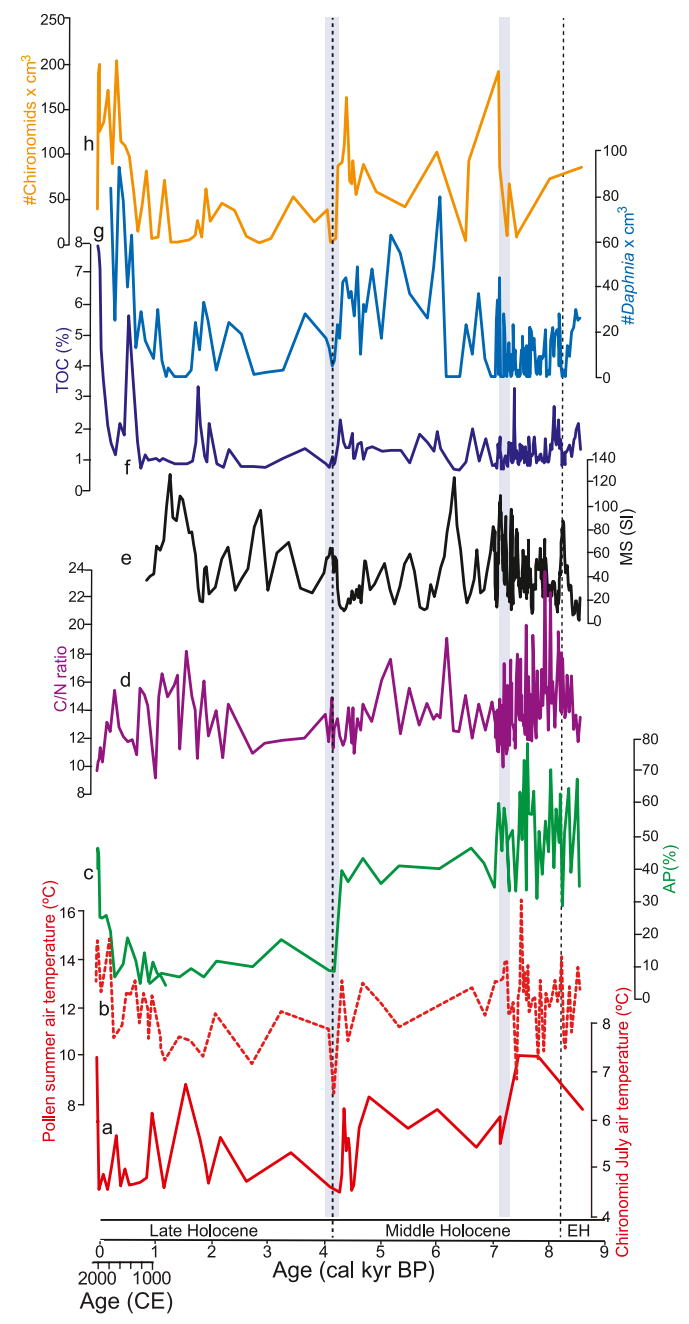


Fig. 6. Comparison of the chironomid-inferred July air temperature (A) with other proxies from LdlMo. (B) Pollen-inferred summer (June, July and August) air temperatures. (C) Arboreal pollen (AP) percentages from Manzano et al. (2019). (D) Carbon/Nitrogen (C/N) ratios. (E) Magnetic susceptibility (MS) results in SI from Manzano et al. (2019). (F) Total Organic Carbon (TOC) percentages. (G) *Daphnia* ephippia concentration (number of ephippia in 1 cm³) from Manzano et al. (2019). (H) Chironomid concentration (number of chironomid head capsules in 1 cm³). The duration of the Early (EH), Middle and Late Holocene is indicated with dashed vertical lines. The blue vertical shadings highlight the main cooling steps observed in the LdlMo record. (For interpretation of the references to colour in this figure legend, the reader is referred to the Web version of this article.)

macroremains were found in the top 5 cm of the sediment core (Manzano et al., 2019).

4. Results

4.1. Updated age model for LdlMo-13 record

Based on the revised age-depth model, the LdlMo sediments, consisting of alternating layers of clays and sandy clays, began accumulating around the Early-Middle Holocene transition with an oldest calibrated radiocarbon date of 8250 cal yr BP at 181 cm depth (Fig. 2). A radiocarbon date of 34,204 cal yr BP (Table 1) was excluded from the age-depth model, as it is likely too old. This age probably reflects the resedimentation of older organic material. Since the bedrock in the alpine Sierra Nevada lakes consists of mica schist, which is siliceous in nature, we expect no input of "old carbon" from carbonate sources into the lake waters.

This updated age model provides very similar ages to the previous age model from Manzano et al. (2019) based on classical linear interpolation of the radiocarbon results. The accumulation rate of the bottommost part of the record between 181 and 83.8 cm is 0.094 cm/yr, contrasting with the changing but lower mean sedimentation rate of the uppermost 83.8 cm of 0.011 cm/yr.

4.2. Organic elemental composition

TOC values range from 0.6 to 7.9 % and tend to be low, with an average value of 1.4 % (Fig. 3). TOC shows variability throughout most of the record without a clear linear trend, except for the increasing trend observed in the last $\sim\!2000$ years until present. TOC minima below 1 % occurred at $\sim\!8300\text{-}8200$, 7600, 7100-7000, 6400-6300, 4200-4100, 2900-2500, 1500-1300 and 700 cal yr BP. TOC peaks above 3 % are observed at $\sim\!7400$, 1700, 480 cal yr BP and, the highest value of the record (7.9 %) in the youngest sample.

Nitrogen (N) values range from 0.05 % to 0.95 % with an average value of 0.13 %. N values change in a very similar fashion as the TOC (see described patterns above, Fig. 3).

C/N ratios range from 9.1 to 23.7 with an average value of 13.8. The C/N ratios show variability, with values around 11.7 at the bottommost part of the record, which increased up to 22–24 reaching the C/N record maxima between 8000 and 7900 cal yr BP. A decreasing trend occurred then until around 7100 cal yr BP, reaching a minimum value of \sim 10. Values increased afterwards, with two peaks at \sim 6200 and 5200 cal yr BP of 19 and 17.5, respectively. Subsequently, generally low values occurred between \sim 4500 and 2700 cal yr BP, with minima at \sim 4500, 4300, 4150 and 2700 cal yr BP. A general increasing trend followed, with a peak value of 18.1 at around 1500 cal yr BP. A decreasing trend occurred afterwards until present, with two minima below 10 at \sim 980 cal yr BP and in the youngest sample (Fig. 3).

4.3. Chironomid results

Seventeen morphotypes of chironomid taxa were identified in the composite chironomid record, which includes 47 analyzed samples from core LdlMo-13-02 $\,$

and 15 samples from the short core LdlMo-13-S (Fig. 4). Chironomid abundance in 2 cm³ of sediments changed considerably through time, from 1 to 204 head capsules per sample, with an average abundance of 63 (Fig. 6). Overall, abundances were high during the Middle Holocene, decreased at 4300 cal yr BP and remained low during the Late Holocene until 500 cal yr BP, when an increase occurred until present. Minima in chironomid abundance were reached at 7400-7250, 6500, 4200, 3050-2600, 1650-1250 cal yr BP (Fig. 6).

Micropsectra radialis type, *Pseudodiamesa* sp. type, *Diamesa* sp. type, *Psectrocladius sordidellus* type, and *Corynoneura arctica* type are the most abundant taxa in the sedimentary record (Fig. 4). Notable changes were

observed in these and other less abundant taxa, allowing us, through visual observation, to distinguish the following periods.

Early-Middle Holocene (8500-7100 cal yr BP)

Micropsectra radialis type dominates the oldest part of the sequence between 8500 and 8000 cal yr BP with abundances around 90 %. Heterotrissocladius marcidus type, Metriocnemus type, Corynoneura arctica type, Diamesa sp. type and Pseudodiamesa sp. type complete the rest of the assemblage (Fig. 4).

Diamesa sp. type, Pseudodiamesa sp. type and Psectrocladius sordidellus type increased considerably between 8000 and 7100 cal yr BP generating minima in Micropsectra radialis type.

Middle Holocene (7100-4200 cal yr BP)

Abundant *Micropsectra radialis* type around 80 %, *Diamesa* sp. type, *Pseudodiamesa* sp. type and *Corynoneura arctica* type, *Psectrocladius sordidellus* type and in less abundance *Cricotopus* sp. type characterized this period.

A minimum of *Micropsectra radialis* type and a peak in *Diamesa* sp. type occurred at 6500 cal yr BP during a minimum in chironomid concentration.

Late Holocene (4200 to −5 cal yr BP)

Psectrocladius sordidellus type and Corynoneura arctica type vanished at the Middle-Late Holocene boundary and only reappeared in one sample, together with cf. Eukiefferiella type at ~1700 cal yr BP. Micropsectra radialis type shows several oscillations but generally decreased with respect to the Early and Middle Holocene with a mean value around 60 %. Three minima in Micropsectra radialis type occurred at ~3050, 1650 and 1000 cal yr BP, coinciding with maxima in Pseudodiamesa sp. and Diamesa sp. and minima in chironomid concentration. Pseudodiamesa sp. type shows an increasing trend in this period until around 1600 cal yr BP, and then a decreasing trend until present.

Modern Climate Warming (MCW) (-5 to -63 cal yr BP; 1955–2013 CE)

Two new taxa, *Micropsectra contracta* type and *M. lindrothi* type appeared during this period. *Psectrocladius sordidellus* type, *Corynoneura arctica* type and *Metriocnemus* type also reappeared then. *Micropsectra radialis* type and *Pseudodiamesa* sp. type decreased in this period.

4.4. Chironomid-inferred summer temperature results

Chironomid-inferred July air temperatures (n = 43) oscillate between 4.7 and 7.3 °C with a mean value of 5.6 °C (Fig. 5). Estimated temperatures during the Early-Middle Holocene (8500-7100 cal yr BP) are high, with a mean value of 6.5 °C and the highest recorded temperatures slightly above 7.3 °C between 7800 and 7400 cal yr BP. A drop of almost 2 °C in temperatures to 5.6 °C occurred at \sim 7100 cal yr BP.

Temperatures stabilized around 6 °C during the rest of the Middle Holocene and a second drop, anticipated by a minimum at $\sim\!4500$ cal yr BP, happened at $\sim\!4200$ cal yr BP. Temperatures remained generally low and around 5.2 °C during the Late Holocene, interrupted by a warming trend that started at $\sim\!2300$ cal yr BP, reaching maximum temperatures around 6.8 °C at $\sim\!1600$ cal yr BP, and around 6.2 °C at $\sim\!1000$ cal yr BP. Minimum temperatures around 4.7 °C are recorded during the Little Ice Age (LIA) at the beginning at 1200–1350 CE (700-600 cal yr BP) and at the end $\sim\!1800$ CE. A sudden and fast increasing trend in temperatures of $\sim\!2.5$ °C occurred since 1955 CE reaching 7.3 °C at present.

4.5. Pollen-inferred summer temperature results

Pollen-inferred summer (June, July, August) air temperatures (n = 75) oscillate between 8.5 and 16.4 $^{\circ}\text{C}$ with a mean value of 12.2 $^{\circ}\text{C}$ (Fig. 5). Estimated temperatures during the Early-Middle Holocene (8500-7100 cal vr BP) show some oscillations but are generally high, with a mean value of 12.4 °C and the highest recorded temperature of 16.4 °C occurred at ~7500 cal yr BP. A significant drop of almost 7 °C in temperatures down to 9 $^{\circ}$ C occurred at \sim 7300 cal yr BP. Temperatures stabilized around 12 $^{\circ}\text{C}$ during the rest of the Middle Holocene and a second drop occurred in two steps, with a first minimum at \sim 4500 cal yr BP and at a second one down to 8.5 $^{\circ}\text{C}$ at ${\sim}4200$ cal yr BP. Temperatures remained around 11 °C during the Late Holocene, but a warming trend started at ~1000 cal yr BP, reaching maximum temperatures around $13\,^{\circ}\text{C}$ at \sim 650 cal yr BP. A minimum around $11\,^{\circ}\text{C}$ is reached afterwards between 400 and 250 cal yr BP (1550-1700 CE), during the Little Ice Age (LIA). A further increase in temperatures of \sim 3.8 $^{\circ}$ C occurred since 1770 CE with temperature estimations around 14 °C until present.

5. Discussion

Chironomid assemblages in lakes at different elevations are closely linked to mean summer air and surface water temperatures (Heiri et al., 2011; Eggermont and Heiri, 2012). Fossil assemblages from high-elevation lakes are particularly sensitive to climate variations, especially summer air and water temperatures, for most biological activity and adult chironomid emergence, completing the life cycle, occur when the lakes are ice-free (Walker, 2001), a period which in high-elevation lakes mostly consists of the summer months. Chironomids exist for the longest part of their life cycle as larvae, which for some species can overwinter in the sediments and then pupate and emerge as adults in spring-summer (Brooks et al., 2007). In a previous study, Jiménez-Moreno et al. (2023) showed the high sensitivity of chironomids from an alpine record from the Sierra Nevada [Laguna de Río Seco (LdRS) record] to temperature change during the past 20,000 years, with a particular focus on temperature changes during the Holocene. Because the chironomid-inferred reconstruction is done using the calibration dataset and transfer function from the Swiss Alps and Norway, these temperature estimations must be interpreted with some caution. Even though the reconstruction is performed using the same chironomid taxa occurring in Sierra Nevada, the Alps or Norway, the calibration functions generally work better in the area where the data sets were developed (Heiri et al., 2011), as local faunistic data provide a more accurate relationship between the species and their local environment. However, the analogue quality statistics obtained for the fossil-modern chironomid comparison indicates that the model accurately represents the data, leading to reliable estimations.

In general terms, the Holocene chironomid assemblages from LdlMo, dominated by Micropsectra radialis type (Fig. 4), are different than the ones from the nearby LdRS record that were mostly characterized by Psectrocladius sordidellus type (Jiménez-Moreno et al., 2023), a chironomid taxon that can be dominant in cold lakes but with a very wide distribution (Heiri and Lotter, 2010). The two sites are located at about the same elevation (LdlMo at 2897m a.s.l. and LdRS at 3029m a.s.l.) and the overall chironomid assemblage differences are likely due to the site orientation, since LdlMo is north facing and likely considerably colder while LdRS faces to the south. Additionally, LdlMo is located at the Mulhacén cirque, where a glacier could have occurred in some cold Holocene phases (Oliva el al., 2018; 2019). The chironomid-inferred mean summer temperature results from LdlMo of 5.6 °C (Fig. 5) also show overall colder temperatures than the ones from LdRS with a mean value of 9 °C for the past 8500 years (Jiménez-Moreno et al., 2023, Fig. 7). Possibly the lake also received cold melt or groundwater during parts of the summer months, which could partly explain the cool reconstructed summer temperatures.

The LdlMo chironomid record is characterized by important

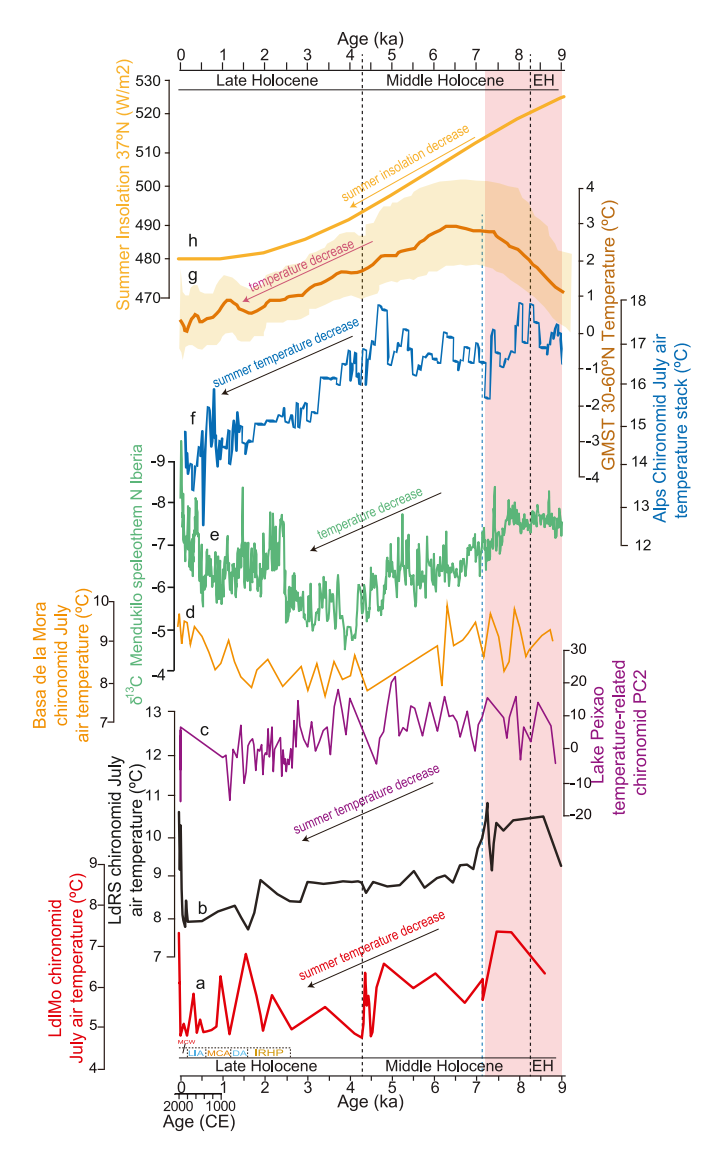


Fig. 7. Comparison of the chironomid-inferred July air temperature from LdlMo (A) with (B) the chironomid-inferred July air temperature from LdRS (Jiménez-Moreno et al., 2023), (C) Lake Peixao temperature-related chironomid PC2 record (Moreno et al., 2023), (D) the chironomid-inferred July air temperature from Basa de la Mora (Tarrats et al., 2018), (E) temperature-related $\delta^{13}\text{C}$ record from Mendukilo speleothem (Bernal-Wormull et al., 2023), (F) a stacked and spliced chironomid-based July air temperature reconstruction from the Alps (Heiri et al., 2015), (G) global mean surface temperature (GMST) composite for 30-60°N (Kaufman et al., 2020), (H) 37°N summer insolation (Laskar et al., 2004). The duration of the Early (EH), Middle and Late Holocene is indicated with dashed vertical lines. IRHP, DA, MCA, LIA and MCW stand for Iberian Roman Humid Period, Dark Ages, Medieval Climate Anomaly, Little Ice Age and Modern Climate Warming. Red shading indicates warmest summer temperatures in LdRS. (For interpretation of the references to colour in this figure legend, the reader is referred to the Web version of this article.)

variability, which is also observed in the sedimentation (e.g., MS, grain size), organic content (e.g., TOC) and characteristics (e.g., C/N) (Fig. 6). Generally, the very detritic intervals (high MS and grain size but low TOC) are characterized by low *Daphnia* and chironomid concentration and dominated by *Diamesa* and *Pseudodiamesa* types (highlighted with blue shading in Fig. 6). *Pseudodiamesa* type is considered one of the coldest-adapted chironomid taxa in the Swiss-Norwegian chironomid lake dataset (Heiri et al., 2011). In the chironomid fossil records from the Alps, *Pseudodiamesa* type often dominates in the coldest periods,

often when *Micropsectra radialis* type is not yet very abundant such as during the period represented in the initial phases of sedimentary deposition right after the region becomes ice free after glacier retreat (Lotter et al., 2006; Ilyashuk et al., 2011; Garcés-Pastor et al., 2022). Therefore, we interpret those more detritic phases as related to coldest conditions, associated with greater physical weathering and erosion, often with less terrestrial and aquatic productivity. This is supported by the chironomid and pollen-inferred summer temperature estimations (Fig. 5) and the pollen record from the LdlMo that generally shows minimum occurrence of forest also pointing to colder climate conditions during those periods (Fig. 6).

In addition to temperature, other environmental factors, such as lake level changes, sedimentary variations and/or changes in productivity should also be considered when interpreting changes in the chironomid assemblages (Rieradevall et al., 1999; Rieradevall and Prat, 1999). While Micropsectra radialis type and Pseudodiamesa are typical lacustrine species, Diamesa types are more common in alpine streams, although Pseudodiamesa may also colonize running water habitats (Rieradevall and Prat, 1999; Moog, 2002). Therefore, variations in lake level and/or fluvial input could also explain, at least partially, the changes in the chironomid assemblages. A lowering of the lake level would generate a more rheophilic environment (or more renewal of the lake water), more detritic sedimentation and less accumulation of chironomid capsules in the sediments and enhanced occurrences of Pseudodiamesa and Diamesa types. However, Diamesa type usually co-occurs with other running water taxa (e.g., Orthocladius type, Eukiefferiella type, other rheophilous orthoclads), which are lacking in the LdlMo sediments, and these would typically be found in traces even at very high elevations in the Alps if stream flow waters contributed to lakes (e.g., Heiri and Lotter, 2003; Lotter et al., 2006). In any event, increases in the lake level would produce the opposite effect - less detritic conditions, and greater abundance of Micropsectra radialis type.

We propose a climatic scenario where variations of both temperature and precipitation control lake level, weathering and runoff oscillations, which in turn, influence the chironomid assemblages. In fact, temperature and precipitation trends from Sierra Nevada generally increase and decrease in unison, shown by the high similarity between the pollen records (proxy for both precipitation and temperature) and chironomid temperature estimations (see Figs. 5 and 6 in this study and Jiménez-Moreno et al., 2023). This way, increased temperature and precipitation can influence higher lake levels, enhanced runoff with terrestrial organic input (as shown by the C/N ratio) and lake productivity, producing a chironomid assemblage indicating warmer climate (e.g., Micropsectra radialis type). The effect of evaporation related to high temperatures in the balance between precipitation/evaporation in this alpine and north-facing lake seems to be low (Anderson et al., 2011). This effect would have been lower than at low elevation Sierra Nevada lakes such as Padul, where low lake levels are recorded during the Early Holocene due to highest summer insolation and very high evaporation (Camuera et al., 2019).

Pollen-based and chironomid-based summer temperature reconstructions indicate a similar temperature development during the Holocene (Fig. 5; Pearson correlation value r = 0.44), supporting that both indicators successfully tracked variations of temperature at LdlMo. However, there are clear differences in the absolute values of reconstructed temperatures between the two indicators, which is also clear at LdRS (Jiménez-Moreno et al., 2023). Pollen estimations show overall higher summer temperatures than the ones obtained by the chironomids (see Figs. 5 and 6). The maximum amplitude of the observed temperature changes is also higher in the pollen than in the chironomid estimations (7.9 °C vs 2.6 °C). Since no local chironomid – temperature calibration dataset is available for southern Spain, chironomid-inferred reconstruction relied on a calibration dataset and transfer function from the Swiss Alps and Norway, and this may partially explain these differences. Even though the reconstruction is done using the same chironomid taxa occurring in Sierra Nevada, the Alps or

Norway, species - temperature relationships may in principle differ to some extent between regions and this could explain systematic offsets in reconstructed temperatures with other temperature indicators. At the same time, chironomids can be expected to largely respond to water temperature (Eggermont and Heiri, 2012), whereas pollen represents terrestrial vegetation and therefore air temperature. Disproportionately colder water temperatures at LdlMo compared with the expected air temperatures, perhaps due to the inflow of cold groundwater or meltwater could therefore also explain why chironomids reconstruct cooler temperatures than pollen. This effect could be exaggerated by the fact that LdlMo is north exposed and can therefore be expected to represent cold microclimatic conditions, whereas pollen is transported to the lake from a much wider source area and will therefore represent different microhabitats and microclimates. Finally, pollen records from alpine lakes such as LdlMo register a regional pollen signal coming from lower elevations and thus reflect warmer temperatures than the very local and colder alpine lake chironomid assemblages. Pollen estimations can also represent large scale altitudinal shifts in all the regional vegetation belts and this can explain why the amplitude of reconstructed temperatures is higher in the pollen than the chironomid-based reconstruction. Therefore, these pollen temperature reconstructions must be interpreted as representing a more regional climatic signal than the chironomid ones. In any event, the most modern pollen-inferred summer temperature data point shows a value of about 13 °C, which seems to agree with the present-day average summer air temperature at the warmer south-facing LdRS site of around 13 °C (Jiménez-Moreno et al., 2023).

Below we discuss the main trends in the chironomid and pollen estimated summer temperature records, comparing them with the sedimentological and geochemical signals from LdlMo and other paleoclimatic records from Sierra Nevada, southern Europe and the Northern Hemisphere during the Holocene.

5.1. Holocene Thermal Maximum (HTM) during the Early and Middle Holocene (8500-7100 cal yr BP)

The LdlMo record shows that the highest temperatures occurred during the Early and Middle Holocene from ~8500 until ~7100 cal yr BP. This is shown in the chironomid record by the occurrence of taxa such as Heterotrissocladius marcidus type and the highest abundance of Psectrocladius sordidellus type, chironomids that are usually not dominating in the coldest mountain lakes (Heiri and Lotter, 2010; Heiri et al., 2011). The pollen record from this time has the highest arboreal pollen (AP) percentages and organic material is characterized by high C/N ratios in the sediments (Fig. 6), interpreted as indicating the greatest forest development in the Sierra Nevada area and highest input of organic matter from a terrestrial vegetation source in LdlMo (Manzano et al., 2019; Jiménez-Moreno et al., 2022, Fig. 6). The similarities of the chironomid-based temperature estimations and the forest development in the LdlMo record (Fig. 6) point to temperature as one of the main drivers controlling vegetation change in the Sierra Nevada. Highest forest abundance indicates the proximity of forest (i.e., treeline) to the alpine wetlands due to upward movement of treeline elevation during climate warming. Therefore, the highest elevation of treeline was reached in the Sierra Nevada subalpine area at this time (Camuera et al., 2019; Jiménez-Moreno et al., 2022).

The LdlMo chironomid-inferred temperature record closely agrees with the nearby LdRS chironomid-deduced summer temperatures also from the Sierra Nevada, which also indicates the HTM in response to highest summer insolation during the Early and Middle Holocene in this area (Jiménez-Moreno et al., 2023, Fig. 7). Other studies also show a maximum in temperature and humidity also occurring in the Sierra Nevada area between ~10,500–7000 cal yr BP (Anderson et al., 2011; Jiménez-Moreno and Anderson, 2012; Mesa-Fernández et al., 2018; Ramos-Román et al., 2018; Jiménez-Moreno et al., 2022; López-Avilés et al., 2022). This is indicated by the highest abundance of tree species pollen and the highest abundance of green aquatic algae (*Botryococcus*

and *Pediastrum*), indicating high lake levels, in those previously studied records

Elsewhere on the Iberian Peninsula (Tarrats et al., 2018, Pyrenees; Moreno et al., 2023; Serra da Estrela; Fig. 7) the HTM is also recorded during the Early and Middle Holocene in other chironomid-based summer temperature records. These also agree with marine temperature estimations, which also show warmest sea surface temperatures (SST) encircling the Iberian Peninsula at that time (Martrat et al., 2014; Rodrigo-Gámiz et al., 2014; Català et al., 2019).

Other regional (Fletcher and Sánchez Goñi, 2008; Bernal-Wormull et al., 2023) and global studies (Jalut et al., 2009; Brayshaw et al., 2011) indicate a warm but also humid Early Holocene, likely driven by peak summer insolation. The so-called Western Mediterranean Humid Period (~10,500–7000 cal yr BP; Toney et al., 2020; García-Alix et al., 2021, 2022) has been attributed to an increased land/sea temperature contrast in fall, enhancing fall/winter rainfall (Tuenter et al., 2003; Meijer and Tuenter, 2007). Additionally, greater North Atlantic moisture advection and a southward storm track shift, linked to prevailing negative NAO-like conditions, contributed to increased regional humidity (Toney et al., 2020; García-Alix et al., 2021, 2022).

5.2. Middle Holocene (7100-4200 cal yr BP)

The LdlMo record shows a rapid drop in the chironomid-inferred temperatures of ~1.7 °C that occurred at ~7100 cal yr BP, which is represented by the decrease and vanishing of some of the chironomid taxa that are usually not found in the coldest mountain lakes (see above) (Figs. 4 and 5) and a decrease in productivity (shown by the TOC, Daphnia and chironomid abundance). The lowered temperatures are also indicated by a decrease in the forest abundance in the Sierra Nevada (see the AP from LdlMo; Fig. 6), which could have been due to cooler temperatures but also due to a decrease in precipitation. Lowered temperature and precipitation are also supported by a decline in lake levels, as seen by the increase in detritic input (MS) and grain size in the LdlMo sediments (Fig. 6). This rapid cooling was also recorded in another chironomid-inferred temperature record from Sierra Nevada at LdRS, where summer temperatures dropped similarly by approximately 1.5 °C around 7000 cal yr BP (Jiménez-Moreno et al., 2023, Fig. 7). These changes appear to be associated to the previously called "7.2 kyr event", the relevance of which starts to be recognized at global scale (e.g., Hou et al., 2023; Pan et al., 2023). This event is also recorded in different records from the Western Mediterranean region. For example, a major drop in sea surface summer temperatures has been described at ~7200 cal yr BP (Jiménez-Espejo et al., 2008) and occurred during the onset of the modern setting of eddies and frontal circulation patterns in the westernmost Mediterranean Sea (Pérez-Folgado et al., 2003). Marine pollen records in the same region and North Africa (Morocco) also show an intense arid period at \sim 7400 \pm 0.2 cal yr BP (Fletcher et al., 2013; Depreux et al., 2022). In parallel, in the North African region African summer rain began to retreat southward (Kuper and Kröpelin, 2006). The forcing of this event could be linked with the summer insolation decrease in the Northern Hemisphere (Laskar et al., 2004; Kaufman et al., 2020, Fig. 7). Although the decrease in insolation is more progressive than the LdlMo record, this cooling could have been enhanced in the Sierra Nevada by other millennial-scale regional mechanisms generating a further temperature drop, such as changes in the North Atlantic subtropical gyre position (Pinho et al., 2025) or the impact of the western Mediterranean thermohaline circulation changes (Fourcade et al., 2024).

The chironomid-inferred temperature records show that temperatures stabilized during the rest of the Middle Holocene (Fig. 7). Similar results are found, for example, in a 1.5 °C cooling from a lake record in the Pyrenees, although it began later, around 6000 cal yr BP (Tarrats et al., 2018). Similar temperature declines at that time have been observed in other chironomid-based reconstructions from Central and Southern European mountain ranges (e.g., Heiri et al., 2015; Toth et al.,

2015; Samartin et al., 2017).

A progressive cooling of more than 2 °C during the Middle and Late Holocene is consistent with global mean surface temperature (GMST) reconstructions (Kaufman et al., 2020, Fig. 7) and closely aligns with both qualitative and quantitative temperature records from southern Europe. This gradual summer cooling was likely driven by a sustained, orbitally induced decline in Northern Hemisphere summer insolation during this period (Laskar et al., 2004, Fig. 7). Coupled with an aridification trend in records from the Sierra Nevada, interpreted as resulting from decreasing winter precipitation, this climatic shift likely contributed to the observed decline in forest cover and lake levels in the study area over the past millennia (Anderson et al., 2011; Jiménez-Moreno and Anderson, 2012; Ramos-Román et al., 2016, 2018; Mesa-Fernández et al., 2018; García-Alix et al., 2018, 2021; Toney et al., 2020; Jiménez-Moreno et al., 2022; López-Avilés et al., 2022; López-Blanco et al., 2024).

5.3. The 4.2 kyr cold event (~4500-4200 cal yr BP)

The Middle Holocene at LdlMo ended with a pronounced temperature decline, occurring in two distinct phases at ~4500 and 4200 cal yr BP. The chironomid-inferred temperature record shows a drop of nearly $2 \,^{\circ}$ C (from 6.5 $^{\circ}$ C to 4.7 $^{\circ}$ C), while the pollen-inferred record indicates a larger decrease of over 4 $^{\circ}$ C (from 13 $^{\circ}$ C to 8.5 $^{\circ}$ C). This climatic shift resulted in the disappearance of chironomid taxa such as *Psectrocladius* sordidellus type (Fig. 4) and the decrease in forest (AP) in the vicinity of LdlMo, of productivity in the lake (e.g., TOC) and terrestrial plant input (C/N) (Fig. 6). This cooling event was possibly associated with the 4.2 kyr event, which has previously been described in other records from the Sierra Nevada as a cold and arid climatic perturbation (Jiménez-Moreno and Anderson, 2012; Ramos-Román et al., 2018; López-Blanco et al., 2025). Regionally, considerable evidence exists of a cold-dry event occurring around 4.2 kyr in southern Spain (Reed et al., 2001; Martín-Puertas et al., 2008; Jalut et al., 2009; Carrión et al., 2010, Carrión, 2002; Jiménez-Moreno et al., 2013) and the Mediterranean area in general (Bini et al., 2019; Di Rita et al., 2022), including one of the coldest events within the Holocene in the chironomid-inferred temperature records from the Pyrenees (Tarrats et al., 2018) and Portugal (Moreno et al., 2023), the Mendukilo temperature-proxy speleothem record (Bernal-Wormull et al., 2023) and the SST record from the Alboran Sea (Català et al., 2019) (Fig. 7).

Although there is ongoing debate on the global extent of this climatic event (McKay et al., 2024) and its characteristics (i.e., cold and/or arid), significant climatic changes occurred at that time, producing profound human societal changes globally (e.g., Weiss, 2016) and marking the Middle-Late Holocene boundary (Walker et al., 2012). Global perturbances that might also be associated with the 4.2 kyr event include cold Bond event 3 (Bond et al., 2001), event 3 of Wanner et al. (2011) and one of the six periods of significant rapid climate change of Mayewski et al. (2004).

However, this cold event is not evident in the chironomid-inferred temperature records from LdRS in the Sierra Nevada or from the Austrian Alps (Jiménez-Moreno et al., 2023; Ilyashuk et al., 2011), where temperatures exhibit a plateau between ~7000-6500 and 3000 cal yr BP (Fig. 7). Perhaps, only especially sensitive, continuous and high-resolution climate proxy records such as the LdlMo were able to register this event in the sedimentary sequences. Alternatively, the differences between LdRS and LdlMo may be attributed to their distinct locations and the contrasting local environments of south-versus north-facing lakes. In LdlMo, chironomid and plant taxa might be more sensitive to temperature, possibly because lake level or precipitation is less limiting than in the south-facing lakes.

The two-phase, LdlMo chironomid-inferred temperature record cooling at \sim 4500 and 4200 cal yr BP agrees well with the high-resolution Padul-15-05 record that also shows multiple cold-dry events at \sim 4500, 4200 and 4000 cal yr BP (Ramos-Román et al.,

2018), indicating that this climatic crisis might have occurred due to multiple cold-dry events at centennial-scale. This characteristic double-peak during this event is recognized in many records from the Iberian Peninsula - from pollen stack compilations (Camuera et al., 2023) to paleohydrological speleothem data (Thatcher et al., 2020) or sea surface temperature records in the Iberian margin (e.g, Català et al., 2019). Recent studies demonstrate that this abrupt climate event had a significant impact in the Iberian prehistory from a cultural, genetic and demographic point of view (Lillios et al., 2016; Jiménez-Espejo et al., 2024). During this event, intense alterations of the landscape by humans and mining pollution can be recognized in South Iberia (Carrión et al., 2007; García-Alix et al., 2013; Alba-Sánchez et al., 2021). The LdlMo chironomid-inferred temperature record is the first to identify and quantify the two-step variability during this event in a continental setting.

5.4. Late Holocene (4200 to -5 cal yr BP)

The LdlMo record shows that temperatures remained generally low during the Late Holocene (Figs. 6 and 7). This is indicated in the chironomid record by the high abundances of the cold taxon *Pseudodiamesa* type, which increased in the Late Holocene (Fig. 4), resulting in generally low values in the summer temperature reconstruction (Fig. 7). Overall, colder conditions during the Late Holocene are also indicated in the LdlMo record by the lowest forest (AP) abundance in the vicinity of the lake and low productivity (TOC, *Daphnia* and chironomid concentration) (Fig. 6)

Our results provide further confirmation of a progressive cooling and aridification trend in the southern Iberian Peninsula, previously shown in the chironomid record from LdRS and the progressive decrease in Mediterranean forest and the increase in herbs and xerophytes (Anderson et al., 2011; Jiménez-Moreno and Anderson, 2012; Jiménez-Moreno et al., 2013, 2022, 2023; Ramos-Román et al., 2016, 2018; Mesa-Fernández et al., 2018; García-Alix et al., 2021, Fig. 6). Overall lake level interpretations at LdlMo (based on the MS and abundances of the rheophilous taxon Diamesa; Figs. 4 and 6) agree with the pollen data, showing an overall lake level decline during the Late Holocene. Although this Late Holocene cooling trend appears to be global in scale (Kaufman et al., 2020), several records from the Iberian Peninsula instead show a warming signal in temperature proxies during this period, including those from Mendukilo Cave and Basa de la Mora in northern Spain (Fig. 7). This may reflect a regional paleoclimatic pattern.

The cooling and aridification during the Late Holocene are linked to a further reduction in summer insolation (Laskar et al., 2004), which may have also contributed to decreased winter rainfall due to a northward shift of the westerlies (García-Alix et al., 2021). This shift, associated with a long-term strengthening of the positive NAO trend, might have led to drier conditions in the region in the past millennia (Olsen et al., 2012).

The overall cool temperatures during the Late Holocene were interrupted by warming between ~2300 and 1600 cal yr BP during part of the Iberian Roman Humid Period (IRHP, 2600-1600 cal yr BP; Martín-Puertas et al., 2009), in agreement with the chironomid record from LdRS (Fig. 7) and other regional records also showing slightly warmer and more humid conditions around that time most-likely due to a persistent negative NAO phase (Jiménez-Moreno et al., 2013; Ramos-Román et al., 2018; López-Avilés et al., 2022; García-Alix et al., 2022; Bernal-Wormull et al., 2023). The inferred temperatures for this warming event in the LdlMo record are seemingly high, when compared to other regional temperature records, but show a similar pattern than the Mendukilo speleothem record from northern Iberia (Fig. 7).

Another warming peak is registered at LdlMo at \sim 1000 cal yr BP during the Medieval Climate Anomaly (MCA) in both the chironomid and pollen estimations. Although the resolution and dating of our record is insufficient to precisely determine the timing and duration of these

temperature variations, our findings align with the previously published LdRS chironomid-based temperature record from Sierra Nevada (Jiménez-Moreno et al., 2023) and other studies suggesting that the Iberian Peninsula experienced relatively warm conditions during the MCA (Moreno et al., 2012). This is further supported by a long-chain diol index (LDI)-derived temperature record from the Sierra Nevada (García-Alix et al., 2021).

Minimum summer temperatures are recorded at \sim 1800 CE during the end of the Little Ice Age (LIA; 1500–1850 CE; Moreno et al., 2012). This agrees with the previous summer temperature reconstruction from LdRS, which also shows a minimum around 1750–1800 CE (Jiménez-Moreno et al., 2023), and other regional temperature reconstructions (Moreno et al., 2012; Ilyashuk et al., 2019).

5.5. Modern Climate Warming (MCW) (-5 to -63 cal yr BP; 1955-2013 CE)

A sudden and rapid increase in temperatures of $\sim 2.5\,^{\circ}\mathrm{C}$ occurred since 1955 CE probably related to anthropogenic climate warming (Figs. 5 and 7). This warming triggered a change in the LdlMo chironomid record with the appearance of two new warm-adapted taxa, *Micropsectra contracta* type and *M. lindrothi* type, and the increase in other warm indicators such as *Psectrocladius sordidellus* type, *Corynoneura arctica* type and *Metriocnemus* type (Fig. 4). The TOC and C/N ratios also show a significant increase in aquatic productivity and algae content at LdlMo in the past decades (Fig. 6), most likely due to warmer temperature (Jiménez et al., 2019).

The rapid temperature rise observed at LdlMo supports the previous temperature estimations from LdRS in the Sierra Nevada (García-Alix et al., 2021), showing a comparable amplitude to the temperature change between the late glacial period and the Early Holocene before the HTM (see Jiménez-Moreno et al., 2023, Fig. 7). Our chironomid-based estimations show temperatures reaching values around 7.3 °C, similar to the HTM (Fig. 7).

It is interesting to note the increase in forest abundance (AP) and pollen temperature estimations from LdlMo in the last ~200 years, with a similar increasing rate as the chironomid-inferred temperatures in the last decades (Fig. 6). Even though this could partially be from the recent vegetation response to climate warming, and the movement of tree taxa towards higher elevations (Jiménez-Olivencia et al., 2016), the main forest species making up for this increase are *Olea* and *Pinus*, which augmented due to human cultivation and reforestation at lower elevations in the Sierra Nevada area (synthesis in Ramos-Román et al., 2019; Jiménez-Moreno et al., 2022).

The rapid rise in temperatures in the last decades is rarely observed in temperature proxies from lake sedimentary records since human impact on the lake sediments can mask this climatic signal, especially at low elevations (e.g., Heiri and Lotter, 2003, 2005; Eggermont and Heiri, 2012). The observation that this warming is recorded in both available chironomid-based temperature reconstructions from the Sierra Nevada demonstrates the robustness of the Sierra Nevada sedimentary records for investigating recent environmental and climate change, as well as the high sensitivity of organisms inhabiting these fragile and unique high-elevation environments to recent warming.

6. Conclusions

The chironomid analysis of the LdlMo sedimentary record provides a Holocene summer air temperature reconstruction, which complements and extends a previous chironomid-based reconstruction from the Sierra Nevada, southern Spain (Jiménez-Moreno et al., 2023). This reconstruction shows highest temperatures (the HTM) in the Early Holocene and Middle Holocene between ~8500 and 7100 cal yr BP, related to the effect of the Early Holocene summer insolation maxima. A reduction in summer insolation generated a cooling that occurred in two major steps: 1) at ~7100 cal yr BP with a rapid drop in the chironomid-inferred

temperatures of $\sim\!1.7$ °C and 2) at $\sim\!4500$ and 4200 cal yr BP, with a significant temperature cooling of almost 2 °C and possibly associated with the global 4.2 kyr event. Temperatures remained generally low during the Late Holocene, but warming was observed between 2300 and 1600 cal yr BP during the IRHP, and around 1000 cal yr BP during the MCA. Minimum temperatures are recorded during the end of the LIA at $\sim\!1800$ CE. A rapid increasing trend in temperatures of $\sim\!2.5$ °C occurred since 1955 CE related to anthropogenic climate warming. This study shows that organisms in alpine ecosystems are responding very sensitively to global warming and further dramatic changes are expected if temperatures continue to rise at the same rate.

Author contributions

G.J.-M. designed the study and wrote the paper. G.J.-M., N.P. and O. H. analyzed the chironomid data and performed the data processing and statistical analysis. J.C. performed the pollen data processing and statistical analysis. A.G.-A., R.S.A., F.J.J.-E. and C.L.-B., helped with data interpretation and writing the paper.

Declaration of competing interest

The authors declare that they have no known competing financial interests or personal relationships that could have appeared to influence the work reported in this paper.

Acknowledgments

This study was supported by projects PID2021-125619OB-C21/C22, funded by the Ministerio de Ciencia e Innovación of Spain, the Agencia Estatal de Investigación and the Fondo Europeo de Desarrollo Regional FEDER MCIN/AEI/10.13039/501100011033/FEDER, UE", grants BIOD22_001 and BIOD22_02, funded by Consejería de Universidad, Investigación e innovación and Gobierno de España and Unión Europea - NextgenerationEU, CGL2013-47038-R, CGL2017-85415-Rand Junta de Andalucía I + D + i Junta de Andalucía 2020 Retos P-20-00059, UGR-FEDER B-RNM-144-UGR18, UGR-FEDER A-RNM-336-UGR20, Project cofinanced by FEDER and LifeWatch-Eric LifeWatch-2019-10-UGR-01 and the research group RNM-190 (Junta de Andalucía). J.C. thanks the Junta Andalucia the postdoctoral for (DGP_POST_2024_00267). RSA acknowledges several travel grants from Northern Arizona University to support this work. We acknowledge the help from Jaime L. Toney (U. Glasgow) and María Calleja recovering the LdlMo sediment cores. This study is a homage to Maria Rieradevall for her latest work on the Pyrenean and Sierra Nevada lake chironomids. We thank the reviewers and the editor Patrick Rioual for their comments improving the manuscript.

Appendix A. Supplementary data

Supplementary data to this article can be found online at https://doi.org/10.1016/j.quascirev.2025.109647.

Data availability

A link to the data and/or code is provided as part of this submission.

References

- Alba-Sánchez, F., Abel-Schaad, D., López-Sáez, J.A., Sabariego-Ruiz, S., Sebastián Pérez-Díaz, S., Luelmo-Lautenschlaeger, R., Garrido-García, J.A., 2021. Early anthropogenic change in western Mediterranean mountains (Sierra Nevada, SE Spain). Anthropocene 33, 100278.
- Anderson, R.S., Jiménez-Moreno, G., Carrión, J.S., Pérez-Martínez, C., 2011. Holocene vegetation history from Laguna de Río Seco, Sierra Nevada, southern Spain. Quat. Sci. Rev. 30, 1615–1629.
- Bernal-Wormull, J.L., Moreno, A., Bartolomé, M., Arriolabengoa, M., Pérez-Mejías, C., Iriarte, E., Osácar, C., Spötl, C., Stoll, H., Cacho, I., Edwards, R.L., Cheng, H., 2023.

- New insights into the climate of northern Iberia during the Younger Dryas and Holocene: the Mendukilo multi-speleothem record. Quat. Sci. Rev. 305, 108006.
- Bini, M., Zanchetta, G., Perşoiu, A., Cartier, R., Català, A., Cacho, I., Dean, J.R., Di Rita, F., Drysdale, R.N., Finnè, M., Isola, I., Jalali, B., Lirer, F., Magri, D., Masi, A., Marks, L., Mercuri, A.M., Peyron, O., Sadori, L., Sicre, M.-A., Welc, F., Zielhofer, C., Brisset, E., 2019. The 4.2 ka BP Event in the Mediterranean region: an overview. Clim. Past 15, 555–577.
- Birks, H.J.B., Braak, C.T., Line, J.M., Juggins, S., Stevenson, A.C., 1990. Diatoms and pH reconstruction. Philos. Trans. R. Soc. Lond. B Biol. Sci. 327, 263–278.
- Bond, G., Kromer, B., Beer, J., Muscheler, R., Evans, M., Showers, W., Hoffmann, S., Lotti-Bond, R., Hajdas, I., Bonani, G., 2001. Persistent solar influence on North Atlantic climate during the Holocene. Science 294, 2130–2136.
- Brayshaw, D.J., Rambeau, C.M.C., Smith, S.J., 2011. Changes in Mediterranean climate during the Holocene: insights from global and regional climate modelling. Holocene 21, 15–31
- Bronk Ramsey, C., 2009. Bayesian analysis of radiocarbon dates. Radiocarbon 51 (1), 337–360
- Brooks, S.J., 2006. Fossil midges (Diptera: Chironomidae) as palaeoclimatic indicators for the Eurasian region. Quat. Sci. Rev. 25, 1894–1910.
- Brooks, S.J., Birks, H.J.B., 2001. Chironomid-inferred air temperatures from Lateglacial and Holocene sites in north-west Europe: progress and problems. Quat. Sci. Rev. 20, 1723–1741.
- Brooks, S.J., Langdon, P.G., Heiri, O., 2007. The identification and use of Palaearctic Chironomidae larvae in palaeoecology. Quat. Res. Associat. Tech. Guide 10, 1–276.
- Camuera, J., Jiménez-Moreno, G., Ramos-Román, M.J., García-Alix, A., Toney, J.L., Anderson, R.S., Jiménez-Espejo, F., Bright, J., Webster, C., Yanes, Y., Carrión, J.S., 2019. Vegetation and climate changes during the last two glacial-interglacial cycles in the western Mediterranean: a new long pollen record from Padul (southern Iberian Peninsula). Quat. Sci. Rev. 205, 86–105.
- Camuera, J., Jiménez-Espejo, F.J., Soto-Chica, J., Jiménez-Moreno, G., García-Alix, A., Ramos-Román, M.J., Ruha, L., Castro-Priego, M., 2023. Drought as a possible contributor to the Visigothic Kingdom crisis and Islamic expansion in the Iberian peninsula. Nat. Commun. 14, 5733.
- Cao, X., Tian, F., Telford, R.J., Ni, J., Xu, Q., Chen, F., Liu, X., Stebich, M., Zhao, Y., Herzschuh, U., 2017. Impacts of the spatial extent of pollen-climate calibration-set on the absolute values, range and trends of reconstructed Holocene precipitation. Ouat. Sci. Rev. 178. 37–53.
- Carrión, J.S., 2002. Patterns and processes of Late Quaternary environmental change in a montane region of Southwestern Europe. Ouat. Sci. Rev. 21, 2047–2066.
- Carrión, J.S., Fuentes, N., González-Sampériz, P., Sánchez Quirante, L., Finlayson, J.C., Fernández, S., et al., 2007. Holocene environmental change in a montane region of southern Europe with a long history of human settlement. Quat. Sci. Rev. 26, 1455–1475.
- Carrión, J.S., Fernández, S., González-Sampériz, P., Gil-Romera, G., Badal, E., Carrión-Marco, Y., López-Merino, L., López-Sáez, J.A., Fierro, E., Burjachs, F., 2010. Expected trends and surprises in the Lateglacial and Holocene vegetation history of the Iberian Peninsula and Balearic Islands. Rev. Palaeobot. Palynol. 162, 458–476.
- Català, A., Cacho, I., Frigola, J., Pena, L.D., Lirer, F., 2019. Holocene hydrography evolution in the Alboran Sea: a multi-record and multi-proxy comparison. Clim. Past 15, 927–942.
- Davis, B.A.S., Chevalier, M., Sommer, P., Carter, V.A., Finsinger, W., Mauri, A., Phelps, L. N., Zanon, M., Abegglen, R., Åkesson, C.M., Alba-Sánchez, F., Anderson, R.S., Antipina, T.G., Atanassova, J.R., Beer, R., Belyanina, N.I., Blyakharchuk, T.A. Borisova, O.K., Bozilova, E., Bukreeva, G., Bunting, M.J., Clò, E., Colombaroli, D., Combourieu-Nebout, N., Desprat, S., Di Rita, F., Djamali, M., Edwards, K.J., Fall, P. L., Feurdean, A., Fletcher, W., Florenzano, A., Furlanetto, G., Gaceur, E., Galimov, A. T., Gałka, M., García-Moreiras, I., Giesecke, T., Grindean, R., Guido, M.A., Gvozdeva, I.G., Herzschuh, U., Hjelle, K.L., Ivanov, S., Jahns, S., Jankovska, V. Jiménez-Moreno, G., Karpińska-Kołaczek, M., Kitaba, I., Kołaczek, P., Lapteva, E.G., Latałowa, M., Lebreton, V., Leroy, S., Leydet, M., Lopatina, D.A., López-Sáez, J.A., Lotter, A.F., Magri, D., Marinova, E., Matthias, I., Mavridou, A., Mercuri, A.M., Mesa-Fernández, J.M., Mikishin, Y.A., Milecka, K., Montanari, C., Morales-Molino, C., Mrotzek, A., Muñoz Sobrino, C., Naidina, O.D., Nakagawa, T., Nielsen, A.B., Novenko, E.Y., Panajiotidis, S., Panova, N.K., Papadopoulou, M., Pardoe, H.S., Pędziszewska, A., Petrenko, T.I., Ramos-Román, M.J., Ravazzi, C., Rösch, M., Ryabogina, N., Sabariego Ruiz, S., Salonen, J.S., Sapelko, T.V., Schofield, J.E., Seppä, H., Shumilovskikh, L., Stivrins, N., Stojakowits, P., Svobodova Svitavska, H., Święta-Musznicka, J., Tantau, I., Tinner, W., Tobolski, K., Tonkov, S., Tsakiridou, M., Valsecchi, V., Zanina, O.G., Zimny, M., 2020. The Eurasian Modern Pollen Database (EMPD), version 2. Earth Sys. Sci. Data 12, 2423-2445.
- Depreux, B., Berger, J.F., Lefèvre, D., Wackenheim, Q., Andrieu-Ponel, V., Vinai, S., Degeai, J.P., El Harradji, A., Boudad, L., Sanz-Laliberté, S., Michel, K., Limondin-Lozouet, N., 2022. First fluvial archive of the 8.2 and 7.6–7.3 ka events in North Africa (Charef River, High Plateaus, NE Morocco). Sci. Rep. 12, 7710.
- Díaz de Federico, A., Puga, E., Burgos, J., Gallegos, J.A., Sanz, de Galdeano, Sanz de Galdeano, C., Crespo, V., Reyes, J.L., 1997. Mapa geológico De La Hoja N° 1027 (Güejar-Sierra). Mapa Geológico De España. E. 1:50.000. Segunda Serie (MAGNA), Primera edición. IGME. Depósito legal: M-39.531-1980.
- Di Rita, F., Michelangeli, F., Celant, A., Magri, D., 2022. Sign-switching ecological changes in the Mediterranean Basin at 4.2 ka BP. Global Planet. Change 208, 102712
- Eggermont, H., Heiri, O., 2012. The chironomid-temperature relationship: expression in nature and palaeoenvironmental implications. Biol. Rev. 87, 430–456.
- Fletcher, W.J., Sanchez Goñi, M.F., 2008. Orbital- and sub-orbital-scale climate impacts on vegetation of the western Mediterranean basin over the last 48,000 yr. Quat. Res. 70, 451–464.

- Fletcher, W.J., Debret, M., Sánchez Goñi, M.F., 2013. Mid-Holocene emergence of a low-frequency millennial oscillation in western Mediterranean climate: implications for past dynamics of the North Atlantic atmospheric westerlies. Holocene 23, 153–166.
- Fourcade, T., Sánchez Goñi, M.F., Lesven, J., Lahaye, C., Philippe, A., 2024. Vegetation response in NW Mediterranean borderlands to the millennial-scale variability of the last glacial period. Quat. Sci. Rev. 334, 108722.
- Garcés-Pastor, S., Coissac, E., Lavergne, S., Schwörer, C., Theurillat, J.-P., Heintzman, P. D., Wangensteen, O.S., Tinner, W., Rey, F., Heer, M., Rutzer, A., Walsh, K., Lammers, Y., Brown, A.G., Goslar, T., Rijal, D.P., nKarger, D.N., Pellissier, L., The, PhyloAlps Consortium, Heiri, O., Alsos, I.G., 2022. High resolution ancient sedimentary DNA shows that alpine plant diversity is associated with human land use and climate change. Nat. Commun. 13, 6559.
- García-Alix, A., Jiménez-Espejo, F.J., Lozano, J.A., Jiménez-Moreno, G., Martínez-Ruiz, F., García Sanjuán, L., Aranda Jiménez, G., García Alfonso, E., Ruiz-Puertas, G., Anderson, R.S., 2013. Anthropogenic impact and lead pollution throughout the Holocene in southern Iberia. Sci. Total Environ. 449, 451–460.
- García-Alix, A., Jiménez-Espejo, F.J., Jiménez-Moreno, G., Toney, J.L., Ramos-Román, M.J., Camuera, J., Anderson, R.S., Delgado Huertas, A., Ruiz, Martínez, Queralt, I., 2018. Holocene geochemical footprint from semi-arid alpine wetlands in southern Spain. Sci. Data 5, 180024.
- García-Alix, A., Camuera, J., Ramos-Román, M.J., Toney, J.L., Sachse, D., Schefuß, E., Jiménez-Moreno, G., Jiménez-Espejo, F.J., López-Avilés, A., Anderson, R.S., Yanes, Y., 2021. Paleohydrological dynamics in the Western Mediterranean during the last glacial cycle. Global Planet. Change 202, 103527.
- García-Alix, A., Jiménez-Moreno, G., Gázquez, F., Monedero-Contreras, R., López-Avilés, A., Jiménez-Espejo, F.J., Rodríguez-Rodríguez, M., Camuera, J., Ramos-Román, M.J., Anderson, R.S., 2022. Climatic control on the Holocene hydrology of a playa-lake system in the western Mediterranean. Catena 214, 106292.
- Grimm, E.C., 1992. Tilia, Version 2. Springfield. IL 62703. Illinois State Museum. Research and Collection Center, USA.
- Hammer, Ø., Harper, D.A.T., Ryan, P.D., 2001. PAST: paleontological statistics software package for education and data analysis. Palaeontol. Electron. 4 (1), 9.
- Heiri, O., Lotter, A.F., 2003. 9000 years of chironomid assemblage dynamics in an alpine lake: long-term trends, sensitivity to disturbance, and resilience of the fauna. J. Paleolimnol. 30 (3), 273–289.
- Heiri, O., Lotter, A.F., 2005. Holocene and Lateglacial summer temperature reconstruction in the Swiss Alps based on fossil assemblages of aquatic organisms: a review. Boreas 34, 506–516.
- Heiri, O.M., Lotter, A.F., 2010. How does taxonomic resolution affect chironomid-based temperature reconstruction? J. Paleolimnol. 44, 589–601.
- Heiri, O., Brooks, S.J., Birks, H.J.B., Lotter, A.F., 2011. A 274-lake calibration data-set and inference model for chironomid-based summer air temperature reconstruction in Europe. Ouat. Sci. Rev. 30, 3445–3456.
- Heiri, O., Ilyashuk, B., Millet, L., Samartin, S., Lotter, A.F., 2015. Stacking of discontinuous regional palaeoclimatic records: Chironomid-based summer temperatures from the Alpine region. Holocene 25, 137–149.
- Hou, M., Wu, W., Cohen, D.J., Zeng, Z., Huang, H., Zheng, H., Ge, Q., 2023. Detection of a mid-Holocene climate event at 7.2 ka BP based on an analysis of globallydistributed multi-proxy records. Palaeogeogr. Palaeoclimatol. Palaeoecol. 618, 111525
- Ilyashuk, E.A., Koinig, K.A., Heiri, O., Ilyashuk, B.P., Psenner, R., 2011. Holocene temperature variations at a high-altitude site in the Eastern Alps: a chironomid record from Schwarzsee ob Sölden, Austria. Quat. Sci. Rev. 30, 176–191.
- Ilyashuk, E.A., Heiri, O., Ilyashuk, B.P., Koinig, K.A., Psenner, R., 2019. The Little Ice Age signature in a 700-year high-resolution chironomid record of summer temperatures in the Central Eastern Alps. Clim. Dyn. 52, 6953–6967.
- IPCC, 2022. In: Pörtner, H.-O., Roberts, D.C., Tignor, M., Poloczanska, E.S., Mintenbeck, K., Alegría, A., Craig, M., Langsdorf, S., Löschke, S., Möller, V., Okem, A., Rama, B. (Eds.), Climate Change 2022: Impacts, Adaptation, and Vulnerability. Contribution of Working Group II to the Sixth Assessment Report of the Intergovernmental Panel on Climate Change. Cambridge University Press.
- Jalut, G., Dedoubat, J.J., Fontugne, M., Otto, T., 2009. Holocene circum-Mediterranean vegetation changes: climate forcing and human impact. Quat. Int. 200, 4–18.
- Jiménez, L., Conde-Porcuna, J.M., García-Alix, A., Toney, J.L., Anderson, R.S., Heiri, O., Pérez-Martínez, C., 2019. Ecosystem responses to climate-related changes in a Mediterranean alpine environment over the last ~ 180 years. Ecosystems 22, 563-577.
- Jiménez-Espejo, F.J., et al., 2008. Detrital input, productivity fluctuations, and water mass circulation in the westernmost Mediterranean Sea since the Last Glacial Maximum. Geochem. Geophys. Geosyst. 9, Q11U02.
- Jiménez-Espejo, F.J., López-Sáez, J.A., Bulian, F., Valiente, S., Giles, F., Ayarzagüena Sanz, M., Garrido-Pena, R., González-Ramón, A., Carrascal, J.M., López-Cidad, F., Barril-Vicente, M., Camuera, J., 2024. Salt production by ignition during the prehistory in the Iberian Peninsula with special focus on the archaeological site of Espartinas (Ciempozuelos, Spain). Quat. Sci. Rev. 336, 108775.
- Jiménez-Moreno, G., Anderson, R.S., 2012. Holocene vegetation and climate change recorded in alpine bog sediments from the Borreguiles de la Virgen, Sierra Nevada, southern Spain. Quat. Res. 77, 44–53.
- Jiménez-Moreno, G., García-Alix, A., Hernández-Corbalán, M.D., Anderson, R.S., Delgado-Huertas, A., 2013. Vegetation, fire, climate and human disturbance history in the southwestern Mediterranean area during the late Holocene. Quat. Res. 79, 110–122.
- Jiménez-Moreno, G., García-Alix, A., Anderson, R.S., Ramos-Román, M.J., Camuera, J., Mesa-Fernández, J.M., Toney, J.L., Jiménez-Espejo, F.J., Carrión, J.S., López-Avilés, A., Rodrigo-Gámiz, M., Webster, C.E., 2022. Reconstruction of past environment and climate using Wetland sediment records from the Sierra Nevada.

- In: Zamora, R., Oliva, M. (Eds.), The Landscape of the Sierra Nevada. Springer, Nature Switzerland AG, pp. 95–114.
- Jiménez-Moreno, G., Heiri, O., García-Alix, A., Anderson, R.S., Jiménez-Espejo, F.J., López-Blanco, C., Jiménez, L., Pérez-Martínez, C., Rodrigo-Gámiz, M., López-Avilés, A., Camuera, J., 2023. Holocene summer temperature reconstruction based on a chironomid record from Sierra Nevada, southern Spain. Quat. Sci. Rev. 319, 108343
- Jiménez-Olivencia, Y., Porcel-Rodríguez, L., Caballero-Calvo, A., Bonet, F.J., 2016. Landuse changes in Sierra Nevada over the last 50 years. Pp.: 56-58. In: Zamora, R., Pérez-Luque, A.J., Bonet, F.J., Barea-Azcón, J.M., Aspizua, R. (Eds.), Global Change Impacts in Sierra Nevada: Challenges for Conservation. Consejería De Medio Ambiente Y Ordenación Del Territorio. Junta de Andalucía.
- Juggins, S., 2014. C2 Version 1.7.6. Software for Ecological and Palaeoecological Data Analysis and Visualisation. Univ. of, Newcastle, Newcastle upon Tyne.
- Kaufman, D., McKay, N., Routson, C., Erb, M., Dätwyler, C., Sommer, P.S., Heiri, O., Davis, B., 2020. Holocene global mean surface temperature, a multi-method reconstruction approach. Sci. Data 7, 201.
- Kuper, R., Kröpelin, S., 2006. Climate-controlled Holocene occupation in the Sahara: motor of Africa's evolution. Science 313, 803–807.
- Laskar, J., Robutel, P., Joutel, F., Gastineau, M., Correia, A.C.M., Levrard, B., 2004.
 A long-term numerical solution for the insolation quantities of the Earth. Astron. Astrophys. 428, 261–285.
- Lillios, K.T., Blanco-González, A., Lee Drake, B., López-Sáez, J.A., 2016. Mid-Late Holocene climate, demography, and cultural dynamics in Iberia: a multi-proxy approach. Quat. Sci. Rev. 135, 138–153.
- Liu, Z., Zhu, J., Rosenthal, Y., Zhang, X., Otto-Bliesner, B.L., Timmerman, A., Smith, R.S., Lohmann, G., Zheng, W., Elison Timm, O., 2014. The Holocene temperature conundrum. Proc. Natl. Acad. Sci. USA 111 (34), E3501–E3505.
- López-Avilés, A., Jiménez-Moreno, G., García-Alix, A., García-García, F., Camuera, J., Anderson, R.S., Sanjurjo-Sánchez, J., Chamorro, C.A., Carrión, J.S., 2022. Postglacial evolution of alpine environments in the western Mediterranean region: the Laguna Seca record. Catena 211, 106033.
- López-Blanco, C., García-Alix, A., Jiménez-Moreno, G., Rodrigo-Gámiz, M., Anderson, R. S., 2024. Climatic fluctuations over the Holocene in southern Iberia (Sierra Nevada, Spain) reconstructed by fossil cladocerans. Palaeogr., Palaeoclimatol. Palaeoecol. 638, 111989.
- López-Blanco, C., García-Alix, A., Sánchez-Almazo, I., Jiménez-Moreno, G., Anderson, R. S., 2025. Holocene changes in moisture source and temperature revealed by the oxygen isotopic composition of fossil *Daphnia* ephippia in Sierra Nevada, southern Spain. Catena 254, 108984.
- Lotter, A.F., Heiri, O., Hofmann, W., van der Knaap, W.O., van Leeuwen, J.F.N., Walker, I.R., Wick, L., 2006. Holocene timber-line dynamics at Bachalpsee, a lake at 2265 m a.s.l. in the northern Swiss Alps. Veg. Hist. Archaeobotany 15, 295–307.
- Luoto, T.P., Kaukolehto, M., Nevalainen, L., 2014. The relationship between water and air temperature in chironomid-based paleoclimate reconstructions: records from boreal and subartic Finland. Holocene 24 (11), 1584–1590.
- Manzano, S., López-Merino, L., Jiménez-Moreno, G., Toney, J.L., Amstrong, H., Anderson, R.S., García-Alix, A., Pérez, J.L.G., Sánchez-Mata, D., 2019.
 A palaeoecological approach to understanding the past and present of Sierra Nevada, a Southwestern European biodiversity hotspot. Global Planet. Change 175. 238–250.
- Martín-Puertas, C., Valero-Garcés, B.L., Mata, M.P., González-Sampériz, P., Bao, R., Moreno, A., Stefanova, V., 2008. Arid and humid phases in southern Spain during the last 4000 years: the Zoñar Lake record, Córdoba. Holocene 18, 907–921.
- Martín-Puertas, C., Valero-Garcés, B.L., Brauer, A., Mata, M.P., Delgado-Huertas, A., Dulski, P., 2009. The Iberian-Roman Humid Period (2600–1600 cal yr BP) in the Zonar Lake varve record (Andalucía, southern Spain). Quat. Res. 71, 108–120.
- Martrat, B., Jimenez-Amat, P., Zahn, R., Grimalt, J.O., 2014. Similarities and dissimilarities between the last two deglaciations and interglaciations in the North Atlantic region. Quat. Sci. Rev. 99, 122–134.
- Mayewski, P.A., Rohling, E.E., Curt Stager, J., Karlén, W., Maasch, K.A., David Meeker, L., Meyerson, E.A., Gasse, F., van Kreveld, S., Holmgren, K., Lee-Thorp, J., Rosqvist, G., Rack, F., Staubwasser, M., Schneider, R.R., Steig, E.J., 2004. Holocene climate variability. Quat. Res. 62, 243–255.
- McKay, N.P., Kaufman, D.S., Arcusa, S.H., Kolus, H.R., Edge, D.C., Erb, M.P., Hancock, C. L., Routson, C.C., Žarczyński, M., Marshall, L.P., Roberts, G.K., Telles, F., 2024. The 4.2 ka event is not remarkable in the context of Holocene climate variability. Nat. Commun. 15, 6555.
- Meijer, P.Th, Tuenter, E., 2007. The effect of precession-induced changes in the Mediterranean freshwater budget on circulation at shallow and intermediate depth. J. Mar. Syst. 68, 349–36.
- Mesa-Fernández, J.M., Jiménez-Moreno, G., Rodrigo-Gámiz, M., García-Alix, A., Jiménez-Espejo, F.J., Martínez-Ruiz, F., Scott Anderson, R.S., Camuera, J., Ramos-Román, M.J., 2018. Vegetation and geochemical response to Holocene rapid climate change in the Sierra Nevada (southeastern Iberia): the Laguna Hondera record. Clim. Past 14, 1687–1706.
- Fauna aquatica austriaca. A comprehensive species inventory of Austrian aquatic organisms with notes. In: Moog, O. (Ed.), 2002. Abteilung Für Hydrobiologie, second ed. Fischereiwirtschaft und Aquakultur der Universität für Bodenkultur, Wien.
- Moreno, A., Pérez, A., Frigola, J., Nieto-Moreno, V., Rodrigo-Gámiz, M., Martrat, B., González-Sampériz, P., Morellón, M., Martín-Puertas, C., Corella, J.P., Belmonte, Á., Sancho, C., Cacho, I., Herrera, G., Canals, M., Grimalt, J.O., Jiménez-Espejo, F., Martínez-Ruiz, F., Vegas-Vilarrúbia, T., Valero-Garcés, B.L., 2012. The medieval climate Anomaly in the Iberian Peninsula reconstructed from marine and lake records. Quat. Sci. Rev. 43 (2012), 16–32.

- Moreno, J., Hernández, A., Raposeiro, P., 2023. Chironomids Principal Coordinates Analysis Temperature Related of Sediment Core PEX19-01, Pangaea. https://doi. org/10.1594/PANGAEA.954426.
- Olsen, J., Anderson, N.J., Knudsen, M.F., 2012. Variability of the North Atlantic Oscillation over the past 5,200 years. Nat. Geosci. 5, 808–812.
- Palacios, D., Gómez-Ortiz, A., Andrés, N., Salvador, F., Oliva, M., 2016. Timing and new geomorphologic evidence of the last deglaciation stages in Sierra Nevada (southern Spain). Quat. Sci. Rev. 150, 110–129.
- Pan, L., Zhao, J., Yang, Y., Wang, K., Pérez-Mejías, C., Cui, J., Dong, X., Zhang, R., Cheng, H., 2023. Different responses of precipitation patterns to the East Asian summer monsoon weakening: the 7.2 and 8.2 ka events. Quat. Sci. Rev. 319, 108329
- Pérez-Folgado, M., Sierro, F.J., Flores, J.A., Cacho, I., Grimalt, J.O., Zahn, R., Shackleton, N., 2003. Western Mediterranean planktonic Foraminifera events and millennial climatic variability during the last 70 kyr. Mar. Micropaleontol. 48, 49–70.
- Pérez-Martínez, C., Tarrats, P., Jiménez-Moreno, G., Prat, N., Rieradevall, M., 2018. Evaluación y seguimiento del cambio global en la Laguna de la Mosca (Sierra Nevada, Granada). Indicadores biológicos. In: Proyectos De Investigación En Parques Nacionales: 2012-2015, pp. 327–338.
- Pinho, T.M.L., Yang, H., Lohmann, G., Portilho-Ramos, R.C., Chiessi, C.M., Bahr, A., et al., 2025. Asynchronous poleward migration of the Atlantic subtropical gyres over the past 22,000 years. Geophys. Res. Lett. 52, e2024GL111497.
- Ramos-Román, M.J., Jiménez-Moreno, G., Anderson, R.S., García-Alix, A., Toney, J.L., Jiménez-Espejo, F.J., Carrión, J.S., 2016. Centennial-scale vegetation and North Atlantic oscillation changes during the late Holocene in the western mediterranean. Quat. Sci. Rev. 143, 84–95.
- Ramos-Román, M.J., Jiménez-Moreno, G., Camuera, J., García-Alix, A., Anderson, R.S., Jiménez-Espejo, F.J., Carrión, J.S., 2018. Holocene climate aridification trend and human impact interrupted by millennial and centennial-scale climate fluctuations from a new sedimentary record from Padul (Sierra Nevada, southern Iberian Peninsula). Clim. Past 14, 117–137.
- Ramos-Román, M.J., Jiménez-Moreno, G., Anderson, R.S., García-Alix, A., Camuera, J., Mesa-Fernández, J.M., Manzano, S., 2019. Climate controlled historic olive tree occurrences and olive oil production in southern Spain. Global Planet. Change 182, 102996.
- Reed, J.M., Stevenson, A.C., Juggins, S., 2001. A multi-proxy record of Holocene climatic change in southwestern Spain: the Laguna de Medina, Cádiz. Holocene 11, 707–719.
- Reimer, P., Austin, W., Bard, E., Bayliss, A., Blackwell, P., Bronk Ramsey, C., Talamo, S., 2020. The IntCal20 northern hemisphere radiocarbon age calibration curve (0–55 cal kBP). Radiocarbon 62 (4), 725–757.
- Rieradevall, M., Prat, N., 1999. Chironomidae from high mountain lakes in Spain and Portugal. In: Hoffrichter, Odwin (Ed.), Lato 20th Century Research on Chironomidae: an Anthology from the 13th International Symposium on Chironomidae. Shaker Verlag, Aachen, pp. 605–613.
 Rieradevall, M., Bonada, N., Prat, N., 1999. Substrate and depth preferences of
- Rieradevall, M., Bonada, N., Prat, N., 1999. Substrate and depth preferences of macroinvertebrates along a transect in a Pyrenean high mountain lake (Lake Redó, NE Spain). Limnética 17, 127–134.
- Rieradevall, M., Brooks, S.J., 2001. An identification guide to subfossil Tanypodinae larvae (Insecta: Diptera: Chironomidae) based on cephalic station. J. Paleolimnol. 25. 81–99.
- Rodrigo-Gámiz, M., Martínez-Ruiz, F., Rodríguez-Tovar, F.J., Jiménez-Espejo, F.J., Pardo-Igúzquiza, E., 2014. Millennial- to centennial-scale climate periodicities and forcing mechanisms in the westernmost Mediterranean for the past 20,000 year. Quat. Res. 81, 78–93.

- Samartin, S., Heiri, O., Joos, F., Renssen, H., Franke, J., Brönnimann, S., Tinner, W., 2017. Warm Mediterranean mid-Holocene summers inferred from fossil midge assemblages. Nat. Geosci. 10, 207–212.
- Schmidhauser, N.R.M.M., Finsinger, W., Cagliero, E., Heiri, O., 2024. Holocene ecosystem and temperature development inferred from invertebrate remains in Zminje Jezero (Dinaric Alps, Montenegro). J. Paleolimnol. 72, 343–361.
- Simpson, G.L., 2007. Analogue methods in palaeoecology: using the analogue package. J. Stat. Software 22, 1–29.
- Snowball, I., Sandgren, P., 2001. Application of Mineral Magnetic Techniques to Paleolimnology. Tracking Environmental Change Using Lake Sediments, vol. 2. Kluwer Academic Publishers, Dordretch, pp. 217–237.
- Tarrats, P., Heiri, O., Valero-Garcés, B., Cañedo-Argüelles, M., Prat, N., Rieradevall, M., González-Sampériz, P., 2018. Chironomid-inferred Holocene temperature reconstruction in Basa de la Mora Lake (Central Pyrenees). Holocene 28 (11), 1685–1696
- Telford, R.J., Birks, H.J.B., 2005. The secret assumption of transfer functions: problems with spatial autocorrelation in evaluating model performance. Quat. Sci. Rev. 24, 2173–2179.
- ter Braak, C.J.F., Juggins, S., 1993. Weighted averaging partial least squares regression (WA-PLS): an improved method for reconstructing environmental variables from species assemblages. Hydrobiologia 269, 485–502.
- ter Braak, C.J.F., Juggins, S., Birks, H.J.B., van der Voet, H., 1993. Weighted averaging partial least squares regression (WA-PLS): definition and comparison with other methods for species-environment calibration. Chapter 25. In: Patil, G.P., Rao, C.R. (Eds.), Multivariate Environmental Statistics. North-Holland, Amsterdam.
- Thatcher, D.L., Wanamaker, A.D., Denniston, R.F., Asmeron, Y., Polyak, V.J., Fullick, D., Ummenhofer, C.C., Gillinkin, D.P., Haws, J.A., 2020. Hydroclimate variability from western Iberia (Portugal) during the Holocene: insights from a composite stalagmite isotope record. Holocene 30, 966–981.
- Toney, J.L., García-Alix, A., Jiménez-Moreno, G., Anderson, R.S., Moossen, H., Seki, O., 2020. New insights into Holocene hydrology and temperature from lipid biomarkers in western Mediterranean alpine wetlands. Quat. Sci. Rev. 240, 106395.
- Toth, M., Magyari, E.K., Buczko, K., Braun, M., Panagiotopoulos, K., Heiri, O., 2015. Chironomid-inferred Holocene temperature changes in the South Carpathians (Romania). Holocene 25 (4), 569–582.
- Tuenter, E., Weber, S.L., Hilgen, F.J., Lourens, L.J., 2003. The response of the African summer monsoon to remote and local forcing due to precession and obliquity. Global Planet. Change 36, 219–235.
- Velle, G., Brooks, S.J., Birks, H.J.B., Willassen, E., 2005. Chironomids as a tool for inferring Holocene climate: an assessment based on six sites in southern Scandinavia. Ouat. Sci. Rev. 24, 1429–1462.
- Walker, I.R., 2001. Midges: chironomidae and related Diptera. In: Smol, J.P., Birks, H.J. B., Last, W.M. (Eds.), Tracking Environmental Change Using Lake Sediments, Zoological Indicators, vol. 4. Kluwer Academic Publishers, Dordrecht, pp. 43–66.
- Wanner, H., Solomina, O., Grosjean, M., Ritz, S.P., Jetel, M., 2011. Structure and origin of Holocene cold events. Quat. Sci. Rev. 30, 3109–3123.
- Walker, M.J.C., Berkelhammer, M., Björck, S., et al., 2012. Formal subdivision of the Holocene series/epoch: a discussion paper by a working group of INTIMATE (integration of ice-core, marine and terrestrial records) and the Subcommission on Quaternary Stratigraphy (International Commission on Stratigraphy). J. Quat. Sci. 27, 649–659.
- Weiss, H., 2016. Global megadrought societal collapse and resilience at 4.2-3.9 ka BP across the Mediterranean and west Asia. PAGES Magazine 24 (2), 62–63.
- Wiederholm, T., 1983. Chironomidae of the Holarctic region: keys and diagnoses. P. 1. Larvae. Entomol. Scand.